공학박사학위논문

통합 예측 위험 관리 기반 포텐셜 필드 기법을 이용한 자율 주행 제어 알고리즘 개발

Predicted Potential Risk-based Vehicle Motion Control of Automated Vehicles for Integrated Risk Management

2016 년 2 월

서울대학교 대학원

기계항공공학부

김 규 원

Abstract

Predicted Potential Risk-based Vehicle Motion Control of Automated Vehicles for Integrated Risk Management

Kyuwon Kim

School of Mechanical and Aerospace Engineering

The Graduate School

Seoul National University

In recent years, global passenger vehicle sales exceed 60milion units per year. With the increasing number of vehicles on the road, safety has become a focal issue. In order to deal with the safety issue, a number of active safety systems have been developed in passenger vehicles, such as brae assist system (BAS), adaptive cruise control(ACC), lane keeping control(LKS), and collision mitigation(CM). The functionalities of the systems include the assistance in recognizing hazards on roadway e.g. forward vehicles, obstacles, the unexpected lane departure. Beyond the development of each independent safety system, the integrated safety system has been considered nowadays.

This dissertation describes design, real-time implementation and test of a fully automated driving algorithm for automated driving in complex urban scenarios and motorways with a satisfactory safety level. The proposed algorithm consists of the following three steps: surround recognition, motion planning, and vehicle control. A full recognition of environment is achieved by data fusion and data interpretation based on the dynamic measurements from the environmental sensors. The recognition of vehicle state including longitudinal, lateral velocity, and position, and driving environment is transformed into a risk potential representation based on probabilistic prediction. The surround recognition system consists of three

main modules: object classification, vehicle/non-vehicle tracking and map/lane-based localization. All system modules utilize information from surround sensors close to market such as vision sensors, radars and vehicle sensors. The objective of the motion planning module is to derive an optimal trajectory as a function of time and the surround recognition results. A safety envelope is represented as a complete driving corridor that leads to destination while making sure all objects are either on outside of the left or right corridor bounds. In the case of moving objects such as other traffic participants, their behaviors are anticipated within specific time horizon. The optimal trajectory planning uses the safety envelope as a constraint and computes a trajectory that the vehicle stays in its safe bounds considering driver's pattern and characteristics based on predicted risk potential method.

The performance of the proposed algorithm has been verified via computer simulations and vehicle test. From the simulation and vehicle test results, it has been shown that the proposed automated driving control algorithm enhances safety with respect to the potential risk considering driver acceptability.

Keywords: Vehicle State Estimation, Collision Risk, Probabilistic Prediction, Potential Field, Dynamic Constraints, Driver Acceptability

Student Number: 2011-30197

Contents

List of Tables

List of Figures

Chapter 1

Introduction

1.1 Background and Motivation

Recently, global passenger vehicle sales exceed 60milion units per year, and with the increasing number of vehicles on the road, safety and convenience of the smart vehicle have become a focal issue. Intelligent vehicles and driver support systems have been considered in order to enhance the safety of drivers and passengers with advances in sensing and navigation technologies. In order to deal with the safety issue, a number of active safety systems have been developed in passenger vehicles, for instance, active safety applications, such as vehicle stability control (VSC), adaptive cruise control (ACC), lane keeping assistance (LKA), lane change assistance (LCA) system, collision mitigation (CM) have been extensively researched. The functionalities of the systems include the assistance in recognizing hazards on roadway e.g. forward vehicles, obstacles, the unexpected lane departure. In

order to achieve enhanced safety goal of zero fatalities, many researches have undertaken the task of integrating individual active safety systems to develop an automated driving system. . Beyond the development of each independent safety system, the integrated safety system has been considered nowadays. In this research, we focus on developing a fully automated driving algorithm capable of automated driving in complex scenarios while a chosen sensor configuration is friendlier to current automotive serial production in terms of cost and technical maturity.

Next generation vehicles after five to ten years are believed to feature autonomous driving capabilities; hence requiring radar/lidar scan data processing for obstacle detection, vision processing for lane keeping, path-generation-and-tracking for autonomous steering control, and so on. The functionalities of the systems include the assistance in recognizing hazards on roadway e.g. forward vehicles, obstacles, the unexpected lane departure. Beyond the development of each independent safety system, the integrated safety system has been considered nowadays. An Artificial potential field approach has been successfully implemented for robot motion planning and path tracking so far [Ge 02], and the concept has been applied on an integrated safety system and automated vehicle navigation [Matsumi 13, Shimoda 07].

A state prediction methods have been studied for threat assessment and decision-making function[Polychronopoulos 07, Yi 04]. In order to ensure the future path of the vehicle, states extension and uncertainty evaluation, a sensor fusion based probabilistic prediction method for holistic vehicle states

is developed. The collision probability based on the predicted vehicle states is defined to represent the collision risk between a subject and surround vehicles.

This dissertation presents the risk management strategy using a risk potential field approach based on a probabilistic states prediction focusing on the data relevant to the subject vehicle interacting with the surround vehicles. Dynamic constraints due to steering behavior, side slip and rollover have been considered as the limitation of the desired motion for collision avoidance and lane keeping. In order to guarantee a driver's acceptability, the driver's maneuvering patterns have been considered into the driving control algorithm. The performance of the proposed collision avoidance algorithm has been investigated via closed-loop simulation with the vehicle simulation software, Carsim, and real-time test via a developed test vehicle.

1.2 Previous Researches

In order to deal with the traffic accidents and provide some conveniences for drivers, many kinds of advanced driver assistance system have been studied and developed.

Smart cruise control system was developed for maintaining a set speed and desired clearance with the front vehicle by acceleration control. The system has been applied many kind of vehicle models of global leading automakers with advanced technologies in environmental sensor such as a radar.

An advanced emergency braking system provides an emergency braking for longitudinal collision avoidance. According to the levels of the collision risk, the system provides acoustic warning, haptic vibration, and automated braking. The system is usually equipped on heavy-duty vehicles before, however, as the essential standard of active safety such as Euro-NCAP, it is widely applied on a passenger cars.

LDWS, LKAS which represent a lane departure warning system and lane keeping assistance system, respectively, use a vision sensor for lane keeping and preventing unintended lane departure. LKAS provides yaw moment or motor torque of electric power steering system, and it is more active than LDWS which provides just warning to a driver with haptic vibration of steering wheel, seat belt and audible warning. LDWS is already equipped in many types of vehicles of global automakers, and LKAS with differential braking or motor torque has limited portions than LDWS for the sensitivity of

drivers.

The research trend of advanced driver assistance system focuses on the integration of each ADAS module. For example, the integration of lane keeping and smart cruise control has been investigated in Cadillac, as a name of 'super cruise'. The researches of full automated driving in low speed situation have been conducted in Ford and BMW. The researches of the partial automated driving on highway such as HAVEit project, SARTRE project in Europe were recently published. Rossetter et al. designed an active lane-keeping assistance system to apply an additional guidance force by using a potential field approach [Rossetter 06]. Sattel et al. proposed a path planning algorithm to keep the lane and avoid a collision based on the potential filed approach [Sattel 08]. Naranjo et al. designed a lane change control algorithm which mimics human behaviors during over taking maneuvers using fuzzy logic for autonomous vehicles [Naranjo 08]. Talvala et al. designed an autonomous driving control algorithm combining look-ahead controller and longitudinal controller to travel the reference path [Talvala 11]. Yoon et al. designed a model predictive control(MPC) based navigation algorithm using an active steering control for collision avoidance with obstacles [Yoon 09]. Borrelli et al. proposed a MPC based steering control algorithm to track a predefined desired path while satisfying constraints and evaluated this approach via simulation studies [Borrelli 05]. In [Falcone 07], Falcone et al. presented a MPC based active steering controller for tracking the desired trajectory as close as possible while satisfying various constraints. In this research, the performance of the control algorithm using a nonlinear vehicle

model as a predictive model is compared with that using successive linearized vehicle model via simulation and experiment test. Then, Falcone et al. presented a sufficient stability condition for the predictive active steering control algorithm based on linear time-varying model [Falcone 08]. These approaches mentioned above only focused on the development of a lateral control law. However, there could be a limitation to follow the desired path only with a lateral control based on linear lateral dynamics. In order to integrate the longitudinal control into the linear lateral dynamics, the system inevitably has nonlinearity, and it has much more complexity to find the optimal MPC solution within its boundary. Furthermore, in the designing of driving control algorithm, a real-time performance should be guaranteed for the actual implementation, however, the solution from the complex problem cannot be provided within the fixed calculation time cycle.

1.3 Thesis Objectives

The objectives of the dissertation for the integrated vehicle motion control of automated vehicles for integrated risk management are as follows:

First, we have to determine an appropriate collision risks around an ego vehicle for reducing an unnecessary control which is struggling against a driver's sensitivity. In order to assess the collision risk of a situation, vehicle velocity estimation, vehicle motion prediction and probabilistic risk assessment algorithm were developed.

Second, we should determine the desired motion of the ego vehicle for collision avoidance. The desired motion for collision avoidance via potential field is proposed in the dissertation. The potential functions of the vehicle driving around a subject vehicle are defined to generate repulsive energies which keep the subject vehicle a safety margin from the target vehicle, or lane. A motion control based on predicted motion of a host vehicle and around vehicle and its predicted potential risk has been developed within a dynamic driving envelope. In order to guarantee the safety driving, the dynamic driving envelope has been set to be a boundary of the controlled motion. Yaw rate candidates and longitudinal acceleration candidates are developed within the dynamic driving envelope, considering the stability constraints of the vehicle which should be guaranteed for the lateral stability. The priorities of desired motions for collision avoidance of multi-traffic situation and lane keeping are established by a situation assessment.

In order to evaluate an integrated safety control algorithm, computer simulation was conducted via MATLAB/SIMULINK, and vehicle simulation software, Carsim. The control input from the integrated safety control algorithm has been validated with the driver's command, and finally a real-time validation has been conducted via a developed test vehicle with several driving scenarios.

1.4 Thesis Outline

The proposed automated driving control system is designed as a hierarchical structure: integrated perception of a driving environment, risk assessment and desired motion determination. The first part deals with the estimation and prediction problems of the vehicle state and driving environment. The second part proposes the design of the integrated safety control algorithm, which provides the desired motion for collision avoidance.

For verifying the proposed integrated safety control algorithms and the perception algorithms, the computer simulation was conducted via MATLAB/SIMULINK and CarSim, which is a commercial tool of the Mechanical Simulation Corporation, and the performances of the proposed algorithm have been additionally evaluated via experimental data on a developed test vehicle.

Specifically, Chapter 2 proposes vehicle longitudinal and lateral velocity estimation, vehicle position estimation and prediction. A probabilistic risk assessment is designed to represent collision risks around the subject vehicle based on the estimated sates and prediction.

In Chapter 3, the integrated safety control algorithm is proposed, in order to guarantee collision avoidance, driver's sensitivity, and stability. The desired motion for collision avoidance via potential field is proposed in the study. The potential functions of the vehicle driving around a subject vehicle are defined to generate predicted risk potential energies which keep the subject vehicle a

safety margin from the target vehicle, or lane. The priorities of desired motions for collision avoidance of multi-traffic situation and lane keeping are established by a situation assessment. The dynamic constraint and stability analysis will be conducted for the application on a various driving situation.

In Chapter 4, the closed loop simulations with driver-vehicle-controller system and vehicle tests were conducted to investigate the performance of the proposed control strategy using the vehicle dynamics software CarSim and Maltab/Simulink. The control input from the integrated safety control algorithm is validated with the driver's command, and a real-time validation will be conducted via a developed test vehicle with several driving scenarios. The tests have been conducted on the actual roads for representing complex driving environment and high speed driving environment to show the similarity between the driving characteristics of human drivers and that of the proposed algorithm

The conclusions are presented in Chapter 5, which also includes the summary of the results of the proposed integrated safety control system and the future works to be done.

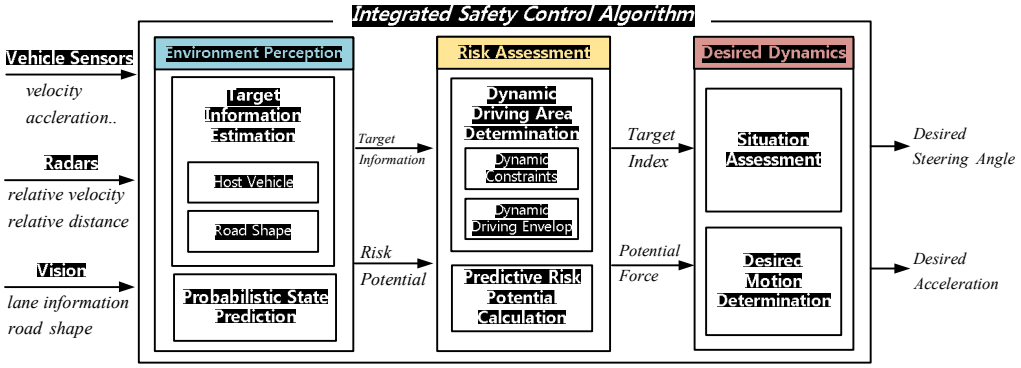

Figure 2. Overall Architecture of Integrated Safety Control Algorithm

Chapter 2

Integrated Perception Algorithm

A human driver recognizes a driving environment via the visual representation from his/her eye and acoustic information. According to the previous research [Althoff 09], the perceptional ability of human drivers is excellent in recognition of an unexpected traffic situation and proper understanding of a traffic situation. Generally, human drivers monitor surrounding environment and predict the future states of surrounding environment based on the current states. Then drivers estimate the threat level of possible actions and decide the maneuver of the subject vehicle in consideration of the predicted states of surrounding vehicles during a finite time-horizon. In order to alternate the visual and acoustic information of human driver, a full recognition of the driving environment should be achieved. For a highly automated driving system, precise information of ego vehicle state and target vehicle such as preceding vehicle, on-coming vehicle, and static obstacles should be estimated. Vehicle status such as longitudinal velocity and lateral velocity are the essential factors for the

safety control which need to be compensated the measured signal from vehicle sensor, or estimated with vehicle sensors. Based on the estimated vehicle status, a safe driving envelope which indicates the drivable boundaries for safe driving over a finite prediction horizon should be determined with the consideration of not only current states of traffic situation surrounding the subject vehicle but also probable future states of that simultaneously [Ferguson 13]. Considering probable future states of surrounding vehicles, it could be expected that the automated driving control algorithm could handle probable risky situation during a finite time-horizon and enhance safety. Furthermore, if we define the safe driving envelope based on the probabilistic prediction, it is expected that an automated driving control algorithm which reflects human driver's driving characteristics with an acceptable ride comfort could be developed.

A schematic diagram for the decision of the safe driving envelope is shown in Figure 2.1. First, vehicle longitudinal velocity and lateral velocity estimation method is described in Section 2.1. The method of the probabilistic prediction of surrounding vehicles is presented briefly in Section 2.2. Then, in Section 5.3, the determination of the desired driving mode and the safe driving envelope is represented.

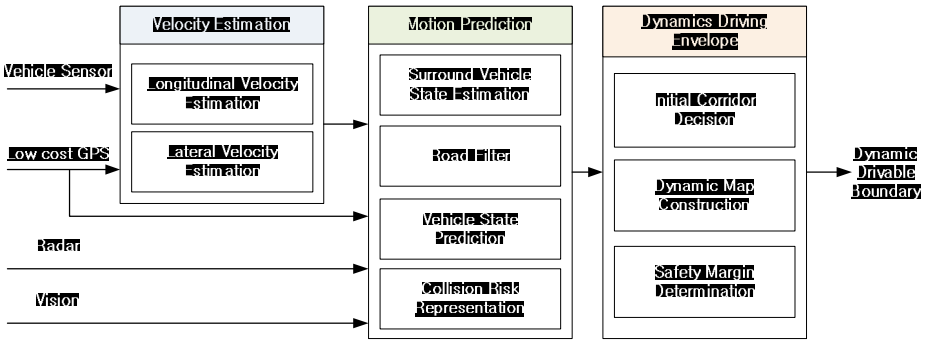

Figure 2.1. Overall Architecture of Integrated Perception Algorithm

2.1 Vehicle Velocity Estimation

Vehicle states are essential information for vehicle safety control and lateral stability control. For its importance, several vehicle states are measured via vehicle sensor which is provided from electronic statbility control (ESC) module. However, the measured signal contains its processing noise and measurement noise, and affected by the external disturbance from the driving situation. In this section, longitudinal velocity measured from the wheel speed sensor has been compensated for guaranteeing a reliabillity, and lateral velocity which is not provided from the vehicle sensor has been estimated using vehicle sensors based on the vehicle dynamics.

2.1.1 Longitudinal Velocity Estimation

Longitudinal velocity of a vehicle can be measured from the wheel speed sensor of electronic stability control (ESC) module. Generally, vehicle longitudinal velocity is calculated with the mean value of the multiplication of two rear wheel rotational speeds and nominal radius of the tire. This kind of estimation method can cover the most cases of driving situation, however, when a driver makes a sudden steering to specific direction, there can be some differences in the left and right wheel speed. As shown in Figure 2.2. This is caused by the difference of the left and right vertical load from the lateral load transfer. Furthermore, when a vehicle drives in the slippery road or sudden acceleration, the wheel speed sensor would provide inaccurate data, because of wheel slip.

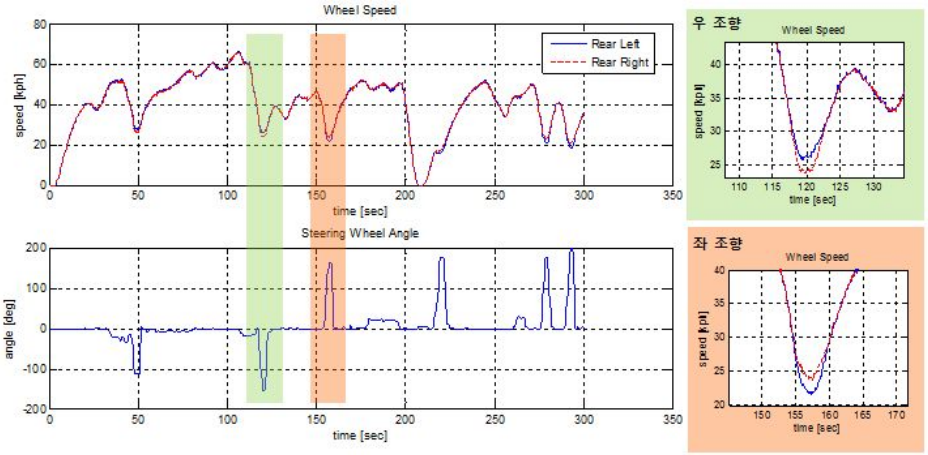

Figure 2.2. Velocity Difference Generated in Sudden Steering Situation

The nominal value of the tire radius can be inaccurate according to the air

pressure, the condition of tire wear, the temperature of the tire. This error would generate a consistent velocity error as shown in Figure 2.3. The average velocity of the two rear tire has consistent error comparing with the high-precision GPS(RT-3002).

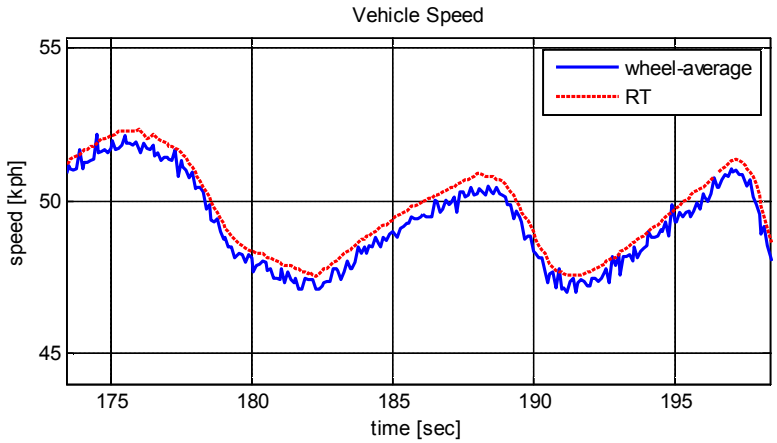

Figure 2.3. Wheel Speed Sensor Characteristic

The bias from the wheel speed sensor can be represented as follows:

$$v_x = \frac{\left(r_{eff} + w_r\right)\cdot\omega_{rl} + \left(r_{eff} + w_r\right)\cdot\omega_{rr}}{2} = \frac{r_{eff}\cdot\left(\omega_{rr} + \omega_{rl}\right)}{2} + w_\omega \qquad (2.1)$$

In order to compensate the error from the averaging method, longitudinal speed estimation method using low cost GPS has been developed. The low cost GPS(U-Blox) has 0.5sec time delay and some dead zone caused by its reception condition comparing with high-precision GPS as shown in the following figures.

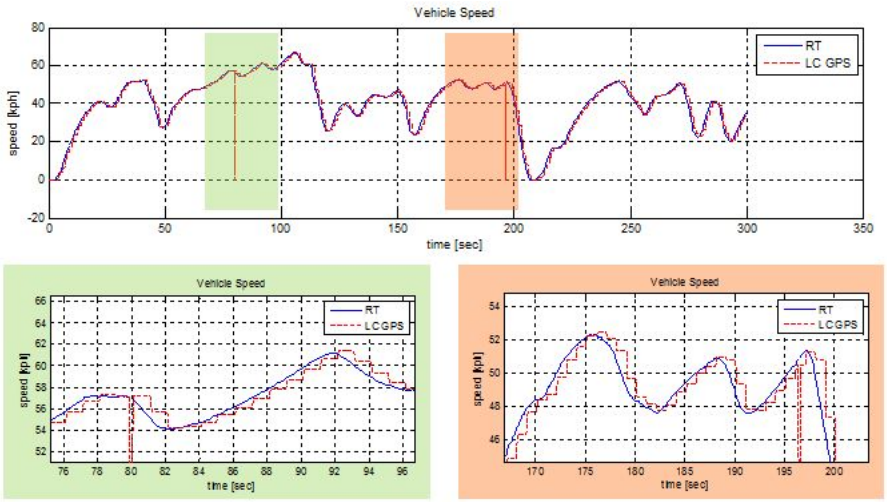

Figure 2.4. Characteristics of Low-Cost GPS

The speed errors from the wheel speed averaging method and low cost GPS are accumulated with vehicle travel distance, and when the vehicle travels 3340m, the position errors from the integration of each velocity are 12m for wheel averaging method, and 5m for the low cost GPS as shown in Figure 2.5.

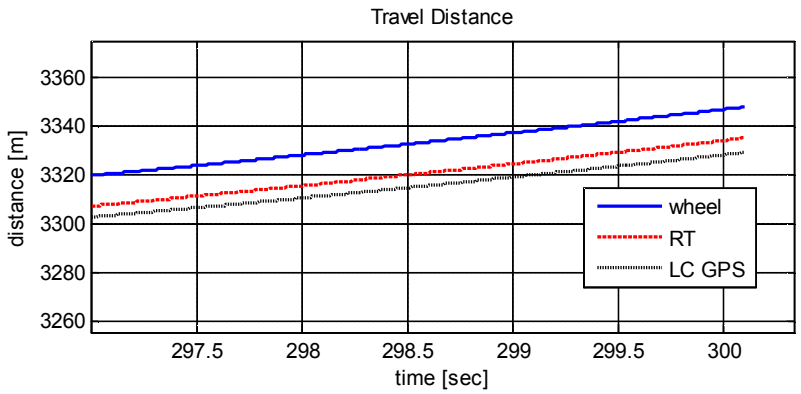

Figure 2.5. Distance Errors of Each Method

In order to compensate the longitudinal velocity error, linear Kalman filter has been used. A vehicle planar model has been used for representing each wheel dynamics of tire as shown in Figure 2.6.

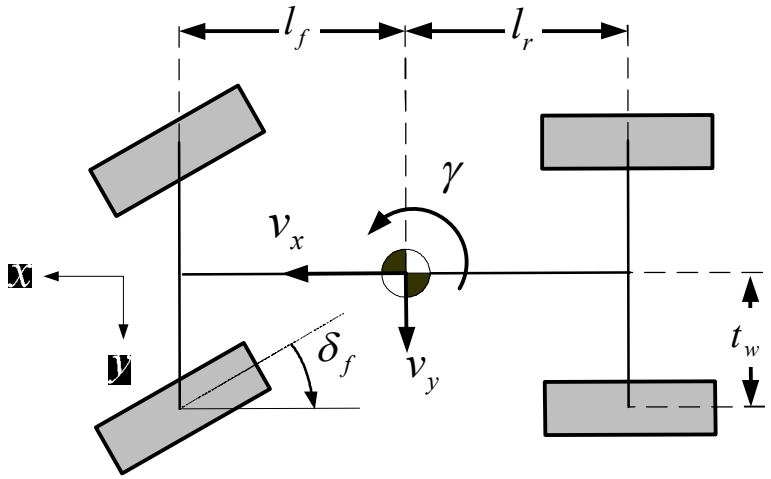

Figure 2.6. Vehicle Planar Model

A state vector contains the longitudinal velocity, the first derivative of the longitudinal velocity, yaw rate, and the first derivative of the yaw rate as shown in following equation:

$$x = \begin{bmatrix} V_x & \dot{V}_x & \gamma & \dot{\gamma} \end{bmatrix}^T$$
$$\dot{x} = \begin{bmatrix} 0 & 1 & 0 & 0 \\ 0 & 0 & 0 & 0 \\ 0 & 0 & 0 & 1 \\ 0 & 0 & 0 & 0 \end{bmatrix} x + \begin{bmatrix} 0 \\ 1 \\ 0 \\ 1 \end{bmatrix} w \tag{2.2}$$

The measurement vector is defined with the yaw rate and the wheel speed of each wheel as shown in Eq.(2.3). The bias of the tire radius is corrected with

the low cost GPS.

$$Z = \begin{bmatrix} \gamma \\ R_{FL} \\ R_{FR} \\ R_{RL} \\ R_{RR} \end{bmatrix} = \begin{bmatrix} \gamma \\ \dfrac{\sqrt{\left(V_x - L\cdot\gamma\right)^2 + \left(t_w\cdot\gamma\right)^2}}{u} \\ \dfrac{\sqrt{\left(V_x + L\cdot\gamma\right)^2 + \left(t_w\cdot\gamma\right)^2}}{u} \\ \dfrac{V_x - L\cdot\gamma}{u} \\ \dfrac{V_x + L\cdot\gamma}{u} \end{bmatrix} + \nu = h(X) + \nu \tag{2.3}$$

Because of the nonlinearity of the measurement matrix, an extended Kalman filter(EKF) method has been applied. The continuous time dynamics of the system has been transformed into discrete time system as follows:

$$x = \begin{bmatrix} v_x & \dot{v}_x & \gamma & \dot{\gamma} \end{bmatrix}^T$$

$$\dot{x} = \begin{bmatrix} 0 & 1 & 0 & 0 \\ 0 & 0 & 0 & 0 \\ 0 & 0 & 0 & 1 \\ 0 & 0 & 0 & 0 \end{bmatrix} x + \begin{bmatrix} 0 \\ 1 \\ 0 \\ 1 \end{bmatrix} w \quad \Rightarrow \quad \mathrm{X}(k+1) = \Phi_d \cdot \mathrm{X}(k) + \Gamma_d \cdot w(k)$$

$$\Phi_d = \begin{bmatrix} 1 & T & 0 & 0 \\ 0 & 1 & 0 & 0 \\ 0 & 0 & 1 & T \\ 0 & 0 & 0 & 1 \end{bmatrix}, \ \Gamma_d = \begin{bmatrix} \dfrac{T^2}{2} \\ T \\ \dfrac{T^2}{2} \\ T \end{bmatrix} \tag{2.4}$$

Then, a time propagation and measurement update process in each time step have been conducted as following step:

Time Propagation

$$\hat{x}_k^- = f_d\left(\hat{x}_{k-1}, u_{k-1}\right) \tag{2.5}$$
$$\hat{z}_k = h\left(\hat{x}_k^-, u_{k-1}\right)$$

Measurement Update

$$K_k = P_k^- \cdot H_k \cdot \left(H_k^T \cdot P_k^- \cdot H_k^T + R \right)^{-1}$$

$$P_k = (I - K_k \cdot H_k) \cdot P_k^-$$

$$\hat{x}_k = f_d(\hat{x}_{k-1}, u_{k-1}) + K_k \cdot \left(z_k - \hat{z}_k \right)$$

$$\textit{where, } P_k^- = A_k \cdot P_{k-1} \cdot A_k^T + Q$$

H matrix in the above equation represents the linearized measurement matrix which can be calculated using the partial derivatives of each state.

$$H = \frac{\partial h}{\partial x} = \begin{bmatrix} \frac{\partial h_1}{\partial x_1} & \frac{\partial h_1}{\partial x_2} & \frac{\partial h_1}{\partial x_3} & \frac{\partial h_1}{\partial x_4} \\ \frac{\partial h_2}{\partial x_1} & \frac{\partial h_2}{\partial x_2} & \frac{\partial h_2}{\partial x_3} & \frac{\partial h_2}{\partial x_4} \\ \frac{\partial h_3}{\partial x_1} & \frac{\partial h_3}{\partial x_2} & \frac{\partial h_3}{\partial x_3} & \frac{\partial h_3}{\partial x_4} \\ \frac{\partial h_4}{\partial x_1} & \frac{\partial h_4}{\partial x_2} & \frac{\partial h_4}{\partial x_3} & \frac{\partial h_4}{\partial x_4} \end{bmatrix} \tag{2.6}$$

The estimation result is shown in Figure 2.7. The accumulated distance error from the proposed estimation method shows the minimum accumulated error comparing with the wheel speed averaging method and only using low cost GPS. In the same travel distance, the accumulated distance error of the proposed method is shown to be 3m with no dead zone shown in Figure 2.7.

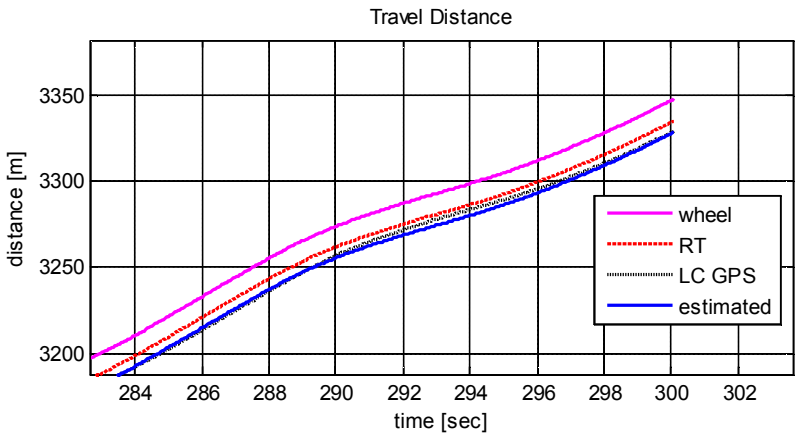

Figure 2.7. Estimated Travel Error of Each Method

2.1.2 Lateral Velocity Estimation

Lateral velocity information is required for vehicle safety control which is not provided from vehicle sensor, and should be estimated. In the previous research, the lateral velocity or body slip angle estimator had been designed based on 2 DOF bicycle model using the linear tire model. However, when the wheel slip angle is not in the linear region, the designed estimator cannot provide the satisfied performance due to the modeling error from the linear tire model.

Recently, many researchers have designed the body slip angle estimator to correct cornering stiffness errors of linear tire model. In this dissertation, the estimator of the lateral tire force and the body slip angle, summarized in the previous research [Moustapha 09, Guillaume 06, Ray 97], is introduced. Figure 2.8 describes the overall architecture of the proposed lateral velocity estimator composed of following three parts; vertical force estimation, reference tire model and lateral velocity estimation.

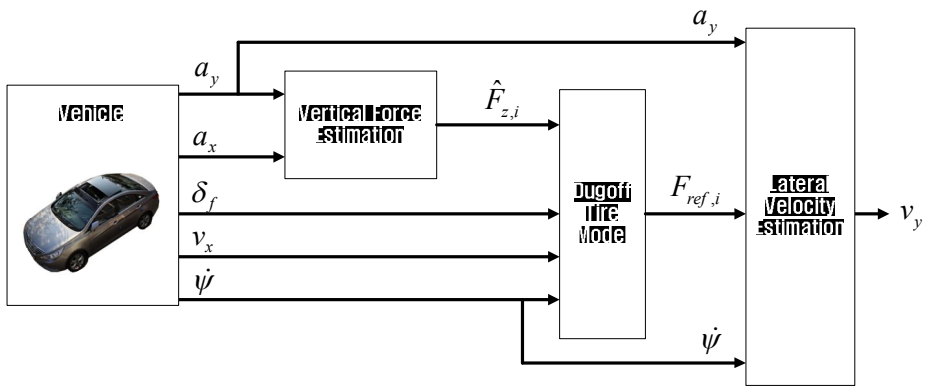

Figure 2.8. Schematic Diagram for Lateral Velocity Estimation

A. Vertical Force Estimation

The vertical tire force information enables to predict the individual maximum tire force on a given tire-road friction coefficient. This implies that the margin of steering and braking force at the individual tires serves as significant information for vehicle stability control. In the true vehicle model, the vertical tire force depends on the suspension dynamics, and it is determined by the driver's maneuvers, such as the throttle, braking, steering input or by the road disturbances. Because of the complexity of the suspension dynamics, and the difficulty in considering the road disturbance, many researchers have simply designed a vertical tire force estimator considering only the driver"s maneuvers, regardless of the road disturbances and the suspension effect, and these have shown good performances for the estimator [Wanki 10]. These estimators have been designed by using the lateral and longitudinal accelerations. In this dissertation, the vertical tire force estimator, summarized in the previous research, is presented. This estimator is designed using the longitudinal and lateral accelerations.

The vertical tire forces can be estimated as follows:

$$\begin{aligned}
\hat{F}_{z,1} &= \frac{1}{2}F_{S,i} - W_{LT,i} - W_{FT,i} \\
\hat{F}_{z,2} &= \frac{1}{2}F_{S,i} + W_{LT,i} - W_{FT,i} \\
\hat{F}_{z,3} &= \frac{1}{2}F_{S,i} - W_{LT,i} + W_{FT,i} \\
\hat{F}_{z,4} &= \frac{1}{2}F_{S,i} + W_{LT,i} + W_{FT,i}
\end{aligned} \tag{2.7}$$

$$where,\ F_{S,i} = \left(m_s \frac{l_r}{l_f + l_r} + m_{uf} \right) g,\ i = 1,2$$

$$F_{S,i} = \left(m_s \frac{l_f}{l_f + l_r} + m_{uf} \right) g,\ i = 3,4$$

where, F_{si} denotes static normal forces at front and rear wheels, $W_{FT,i}$ the longitudinal load transfer, $W_{LT,i}$ the lateral load transfer, respectively. The lateral load transfer can be represented as following:

$$K_{roll}\phi + C_{roll}\dot{\phi} = m_s e_s \left(a_y - g\phi - e_s \ddot{\phi} \right) - I_{xxs}\ddot{\phi}$$

$$W_{LTF} + W_{LTR} = \frac{\left(m_s h_r + m_u h_a \right)}{t} a_y + \frac{K_{roll}\phi + C_{roll}\dot{\phi}}{t} \tag{2.8}$$

$$W_{LTF} + W_{LTR} = \frac{\left(m_s h_r + m_u h_a \right)}{t} a_y + \frac{m_s e_s \left(a_y - g\phi - e_s \ddot{\phi} \right) - I_{xxs}\ddot{\phi}}{t}$$

Where, a_y is lateral acceleration, m_u and m_s mean unsprung mass and sprung mass of the vehicle. K_{roll} and C_{roll} represent suspension stiffness and damping coefficients. Subscript F and R denote front and rear respectively.

B. Reference Tire Model : Dugoff's Tire Model

Dugoff's tire model, as shown in Eq.(2.9), is used as a reference tire model.

$$\bar{F}_{tyi} = C_y \cdot \frac{\tan(\alpha_i)}{1+\lambda_i} \cdot f(\delta_i)$$

$$where,\ \delta_i = \frac{\mu \cdot \hat{F}_{tzi} \cdot (1+\lambda_i)}{2\sqrt{(C_x \cdot \lambda_i)^2 + (C_y \cdot \tan(\alpha_i))^2}} \tag{2.9}$$

$$f(\delta_i) = \begin{cases} (2-\delta_i)\cdot\delta_i & if\ (\delta_i < 1) \\ 1 & if\ (\delta_i \geq 1) \end{cases}$$

where, α_i and λ_i represent denote the slip angle and the slip ratio at each wheel, respectively. The estimator of the lateral tire force and the body slip angle is designed based on 2-DOF bicycle model and the relaxation tire model as shown in following figure [Rajesh 06].

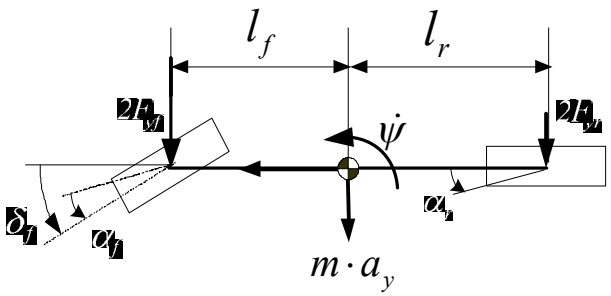

Figure 2.9. 2-DOF bicycle model

The dynamic equation of the 2 DOF bicycle model is expressed as follows:

$$m \cdot a_y = m(\dot{v}_y + v_x \cdot \gamma) = 2 \cdot F_{tyf} \cdot \cos(\delta_f) + 2 \cdot F_{tyr}$$

$$\dot{v}_y = \frac{2 \cdot F_{tyf} \cdot \cos(\delta_f) + 2 \cdot F_{tyr}}{m} - v_x \cdot \gamma \tag{2.10}$$

$$= \frac{2 \cdot x_3 \cdot \cos(u_2) + 2 \cdot x_4}{m} - u_1 \cdot \gamma = f_1(x,u)$$

$$I_z \cdot \dot{\gamma} = 2 \cdot l_f \cdot F_{tyf} \cdot \cos(\delta_f) - 2 \cdot l_r \cdot F_{tyr}$$

$$\dot{\gamma} = \frac{2 \cdot l_f \cdot F_{tyf} \cdot \cos(\delta_f) - 2 \cdot l_r \cdot F_{tyr}}{I_z}$$

$$= \frac{2 \cdot l_f \cdot x_3 \cdot \cos(u_2) - 2 \cdot l_r \cdot x_4}{I_z} = f_2(x,u)$$

The relaxation tire model is used to consider transient behavior of lateral tire force. When vehicle side slip angle changes, a lateral tire force is created with a time lag. This transient behavior of the lateral tire force can be expressed using the relaxation tire model, as following equation.

$$\begin{aligned} \dot{F}_{tyi} &= -\frac{v_x}{\sigma}\left\{F_{tyi} - \bar{F}_{tyi}(\lambda_i, \alpha_i, \hat{F}_{tzi})\right\} \\ &= -\frac{u_1}{\sigma}\left\{x_i - \bar{F}_{tyi}(\lambda_i, \alpha_i, \hat{F}_{tzi})\right\} = f_i(x,u) \qquad where,\ i = 3,4 \end{aligned} \tag{2.11}$$

where, σ denotes the relaxation length. The relaxation length is the distance covered by the tire while the tire force is kicking in [Moustapha 09]. The lateral tire force characteristics from the reference tire model according to the vertical tire force can be represented as following figure.

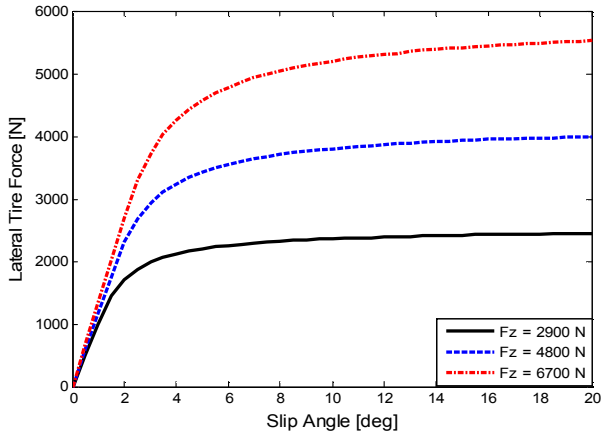

Figure 2.10. Lateral Tire Force Characteristics

C. Lateral Velocity Estimation

The nonlinear state-space representation can be obtained from the dynamic equation of the 2-DOF bicycle model and the relaxation tire model. In the nonlinear state-space representation, the state vector is defined with the lateral velocity, yaw rate and the front and rear lateral tire force, and the input vector comprises the vehicle speed, the front steering angle and the front and rear reference tire forces as follows:

$$\begin{aligned} x &= \begin{bmatrix} v_y & \gamma & F_{tyf} & F_{tyr} \end{bmatrix}^T = \begin{bmatrix} x_1 & x_2 & x_3 & x_4 \end{bmatrix}^T \\ u &= \begin{bmatrix} v_x & \delta_f & \overline{F}_{tyf} & \overline{F}_{tyr} \end{bmatrix}^T = \begin{bmatrix} u_1 & u_2 & u_3 & u_4 \end{bmatrix}^T \end{aligned} \tag{2.12}$$

Using the state and input vectors, the state-space representation can be obtained as follow:

$$\begin{aligned} \dot{x}_1 &= \frac{2 \cdot x_3 \cdot \cos(u_2) + 2 \cdot x_4}{m} - x_2 \cdot u_1 = f_1(x,u) \\ \dot{x}_2 &= \frac{2 \cdot l_f \cdot \cos(u_2) \cdot x_3 - 2 \cdot l_r \cdot x_4}{I_z} = f_2(x,u) \\ \dot{x}_3 &= -\frac{u_1}{\sigma}\{x_3 - u_3\} = f_3(x,u) \\ \dot{x}_4 &= -\frac{u_1}{\sigma}\{x_4 - u_4\} = f_4(x,u) \end{aligned} \tag{2.13}$$

The measurement states are yaw rate and the lateral acceleration from vehicle sensor represented as follows:

$$z_k = \begin{bmatrix} \gamma \\ a_y \end{bmatrix} = \begin{bmatrix} x_2 \\ \dfrac{2 \cdot \cos(\delta_f) \cdot x_3 + 2 \cdot x_4}{m} \end{bmatrix} + v_k = h\left(x_k, u_k\right) + v_k \tag{2.14}$$

Continuous-time systems in above equations can be transformed into discrete time system using zero-order hold method, as follows:

$$
\begin{aligned}
x_{k+1} &= x_k + \Delta t \cdot f\left(x_k,\ u_k\right) + w_k \\
&= f_d\left(x_k,\ u_k\right) + w_k \\
z_k &= h\left(x_k, u_k\right) + v_k
\end{aligned}
\tag{2.15}
$$

From the above discrete-time system, the lateral tire force and the body slip angle can be estimated based on the Extended Kalman Filter (EKF) method as follows:

Time Propagation

$$
\begin{aligned}
\hat{x}_k^- &= f_d\left(\hat{x}_{k-1}, u_{k-1}\right) \\
\hat{z}_k &= h\left(\hat{x}_k^-, u_{k-1}\right)
\end{aligned}
\tag{2.16}
$$

Measurement Update

$$
\begin{aligned}
K_k &= P_k^- \cdot H_k \cdot \left(H_k^T \cdot P_k^- \cdot H_k^T + R\right)^{-1} \\
P_k &= (I - K_k \cdot H_k) \cdot P_k^- \\
\hat{x}_k &= f_d(\hat{x}_{k-1}, u_{k-1}) + K_k \cdot \left(z_k - \hat{z}_k\right)
\end{aligned}
$$

where, $P_k^- = A_k \cdot P_{k-1} \cdot A_k^T + Q$

A_k and H_k are linearized state matrix as follows:

$$
\begin{aligned}
A_{[i,j]} &= \left.\frac{\partial f_i}{\partial x_j}\right|_{\hat{x}_{k-1},\, u_{k-1}} \\
&= \begin{bmatrix}
1 & -v_x \cdot \Delta t & \dfrac{\Delta t \cdot \cos\delta_f}{m} & \dfrac{\Delta t}{m} \\
0 & 1 & \Delta t \cdot \dfrac{l_f \cdot \cos\delta_f}{I_z} & -\Delta t \cdot \dfrac{l_r}{I_z} \\
0 & 0 & 1 - \Delta t \cdot \dfrac{v_x}{\sigma} & 0 \\
0 & 0 & 0 & 1 - \Delta t \cdot \dfrac{v_x}{\sigma}
\end{bmatrix}
\end{aligned}
$$

$$H_k = \left.\frac{\partial h_i}{\partial x_j}\right|_{\hat{x}_k^-,\, u_{k-1}}$$

$$= \begin{bmatrix} 0 & 1 & 0 & 0 \\ 0 & 0 & \dfrac{\cos\delta_f}{m} & \dfrac{1}{m} \end{bmatrix}$$

The proposed estimation algorithm has been validated via mathematical simulation using Carsim and Matlab Simulink. A sinusoidal steering angle input has been applied on the vehicle with 60kph velocity as shown in Figure 2.11(a). Lateral velocity from the vehicle model has been confirmed to be well estimated as shown in Figure 2.11(b).

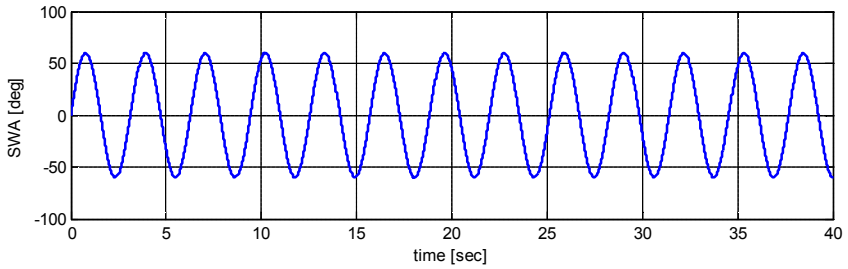

(a) Steering wheel angle command

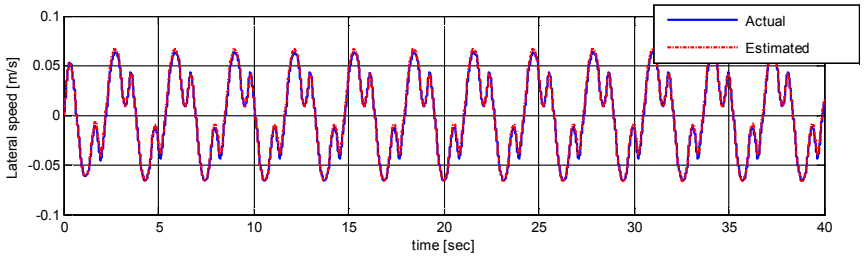

(b) Estimated lateral velocity and actual lateral velocity

Figure 2.11. Simulation Results : Lateral Velocity Estimation

A proposed estimation algorithm has been applied on the test vehicle. The test has been conducted on a test track with single lane change scenario. Vehicle speed and steering command are shown in Figure 2.12, and from the test results, the proposed lateral velocity estimation algorithm is well matched with measured lateral velocity from high-precision GPS (RT-3002) data.

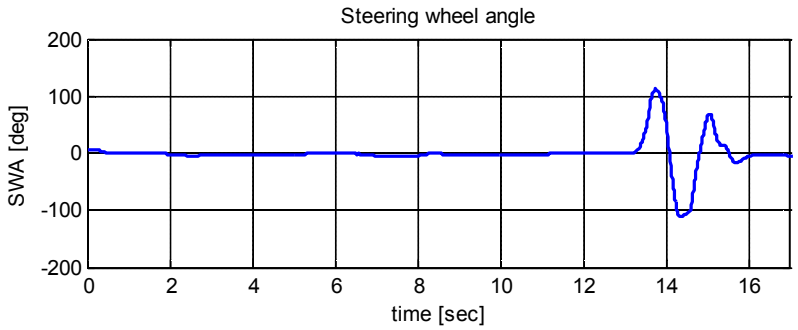

(a) Driver's steering wheel angle

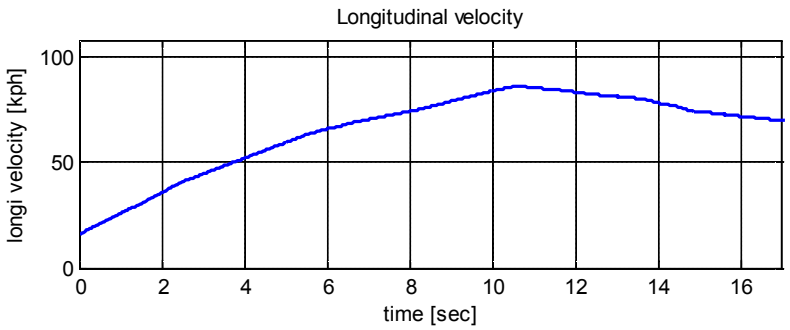

(b) Vehicle longitudinal velocity

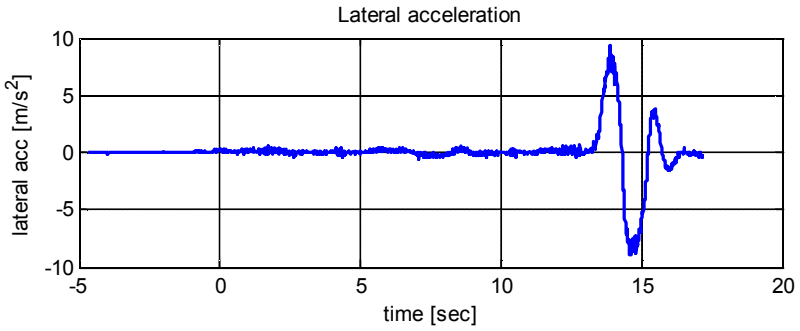

(c) Vehicle lateral acceleration

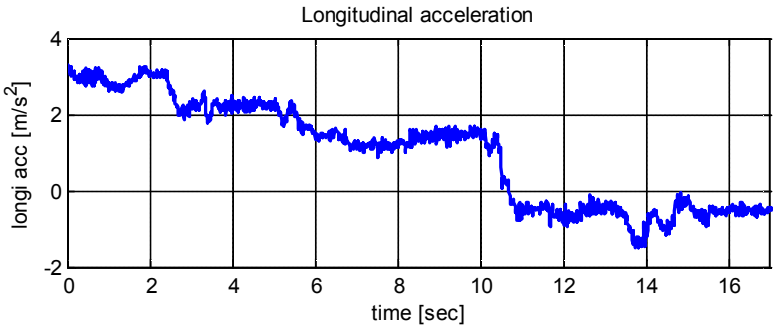

(d) Vehicle longitudinal acceleration

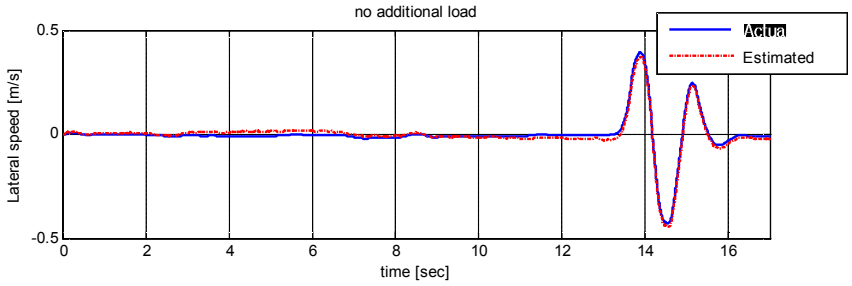

(e) Estimated lateral velocity and measured lateral velocity

Figure 2.12. Vehicle Test Results : Lateral Velocity Estimation

2.2 Perception of Dynamic Driving Environment

Dynamic driving environment recognition consists of three main modules: object classification, vehicle/non-vehicle tracking and lane-based localization. All system modules make use of information from various onboard sensors. The main sensing components are surround sensors such as cameras, radars and vehicle sensors including but not limited to wheel speed and inertia sensors.

A probabilistic state prediction presents the predicted potential states of the subject vehicle and the surrounding vehicles in finite time horizon. The state prediction algorithm consists as shown in the following figure.

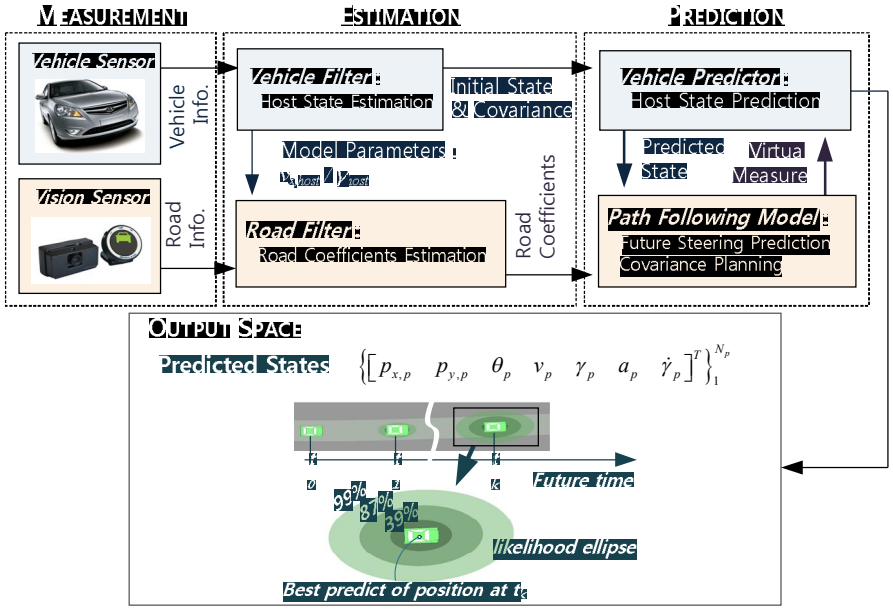

Figure 2.13. Schematic Description of Probabilistic Prediction

2.2.1 Vehicle State Prediction

The Kalman filter is widely used to estimate the states represented in a state space equation. In order to establish a state prediction, the vehicle state estimation method such as longitudinal velocity, yaw rate, longitudinal acceleration and yaw acceleration has been developed [Kim 13].

A road geometry estimation has been established with the measurements from a vision sensor. The road geometry can be described by a 2nd order polynomial [Schwartz 03]. Likewise with the vehicle states estimation, the Kalman filter is used for the estimation of road geometry coefficients of the polynomial.

The state prediction of the vehicle has been established under the assumptions that a subject and surround vehicles maintain current behavior in the finite time horizon. The vehicle position in the finite time horizon is represented as follows:

$$\begin{aligned} x_p[i+1] &= f_p\left(x_p[i]\right) + w_p[i], \qquad i = 0, \cdots, N_p - 1 \\ &= \begin{bmatrix} f_{1,p} & f_{2,p} & f_{3,p} & f_{4,p} & f_{5,p} & f_{6,p} & f_{7,p} \end{bmatrix} + w_p[i] \end{aligned} \tag{2.17}$$

$$x_p = \begin{bmatrix} p_{x,p} & p_{y,p} & \theta_p & v_p & \gamma_p & a_p & \dot{\gamma}_p \end{bmatrix}^T$$

$$f_{1,p} = p_{x,p} + \left(v_p \cos\theta_p\right)\Delta t + \left(a_p \cos\theta_p + \gamma_p v_p \sin\theta_p\right)\frac{\Delta t^2}{2}$$

$$f_{2,p} = p_{y,p} + \left(v_p \sin\theta_p\right)\Delta t + \left(a_p \sin\theta_p + \gamma_p v_p \cos\theta_p\right)\frac{\Delta t^2}{2}$$

$$f_{3,p} = \theta_p + \left(\gamma_p\right)\Delta t + \left(\dot{\gamma}_p\right)\frac{\Delta t^2}{2}$$

$$f_{4,p} = v_p + \left(a_p\right)\Delta t + \left(-k_a a_p\right)\frac{\Delta t^2}{2}$$

$$f_{5,p} = \gamma_p + \left(\dot{\gamma}_p\right)\Delta t + \left(-k_{\dot{\gamma}}\dot{\gamma}_p\right)\frac{\Delta t^2}{2}$$

$$f_{6,p} = a_p + \left(-k_a a_p\right)\Delta t + \left(k_a{}^2 a_p\right)\frac{\Delta t^2}{2}$$

$$f_{7,p} = \dot{\gamma}_p + \left(-k_{\dot{\gamma}}\dot{\gamma}_p\right)\Delta t + \left(k_{\dot{\gamma}}{}^2\dot{\gamma}_p\right)\frac{\Delta t^2}{2}$$

The process noise is assumed to have Gaussian white characteristics including the linearized system covariance as shown in following equations:

$$\begin{aligned} & w_p[i] \sim \left(0, W_p[i]\right) \\ & W_p[i] = \left(B_p \Delta t + F_p[i] B_p \frac{\Delta t^2}{2}\right) Q_p \left(B_p \Delta t + F_p[i] B_p \frac{\Delta t^2}{2}\right)^T \end{aligned} \tag{2.18}$$

$$F_p[i] = \left.\frac{\partial f_p}{\partial x_p}\right|_{x_p = \hat{x}_p[i]} \qquad B_p = \begin{bmatrix} 0 & 0 & 0 & 0 & 0 & 0 & 1 \\ 0 & 0 & 0 & 0 & 0 & 1 & 0 \end{bmatrix}^T$$

The subscript p in Eq.(2.18) denotes 'predictive'. A prediction procedure at the first future time step is depicted as Figure 2.14. The desired yaw rate for lane keeping is supposed to be a virtual measurement as shown in the following equation.

$$
\begin{aligned}
z_p[i] &= H_p \cdot x_p[i] + v_p[i], \qquad i = 0, \cdots, N_p \\
&= \begin{bmatrix} 0 & 0 & 0 & 0 & 1 & 0 & 0 \end{bmatrix} \cdot x_p[i] + v_p[i] \\
&= \overline{\gamma}_{des,p}[i] \\
&= -C \cdot \overline{x}_{e,p}[i] + \gamma_{ff,p}[i]
\end{aligned}
\tag{2.19}
$$

Where,

$$
\begin{aligned}
\overline{x}_{e,p}[i] &= f_e\left(\overline{x}_p[i], \hat{x}_r[0]\right) \\
&= \begin{bmatrix} \overline{e}_y[i] & \overline{e}_\theta[i] & \overline{\gamma}_p[i] \end{bmatrix}^T \\
&= \begin{bmatrix} \overline{p}_{y,p}[i] - \left\{\hat{a}_2 \cdot \overline{p}_{x.p}[i]^2 + \hat{a}_1 \cdot \overline{p}_{x.p}[i] + \hat{a}_0 + \hat{w}_{road} \cdot N[i]\right\} \\ \overline{\theta}_p[i] - \tan^{-1}\left(2\hat{a}_2 \cdot \overline{p}_{x,p}[i] + \hat{a}_1\right) \\ \overline{\gamma}_p[i] \end{bmatrix}
\end{aligned}
$$

$$
v_p[i] \sim \left(0, V_p[i]\right)
$$

$$
V_p[i] = V_{p,const} + \begin{bmatrix} \overline{e}_y[i] & \overline{e}_\theta[i] \end{bmatrix}^T w_{correct} \begin{bmatrix} \overline{e}_y[i] \\ \overline{e}_\theta[i] \end{bmatrix}
$$

The following figures represent the procedure of state prediction. Based on the lane information from camera, road center line can be estimated. The predicted motion of a subject vehicle is propagating according to the future time step with assumption that the subject vehicle keeps its lane. From the vehicle state measurement such as yaw rate, vehicle speed and acceleration, measurement update of the subject state is achieved. The schematic description of the successive sequences can be depicted as:

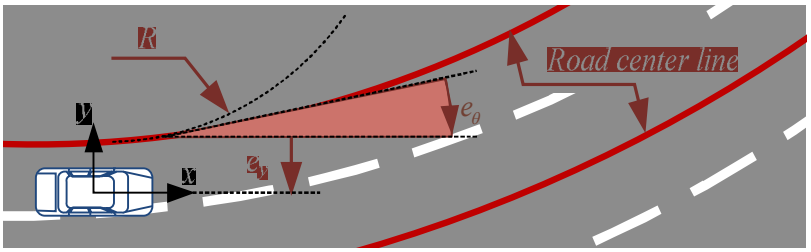

(a) Relationship between the Subject Vehicle and Center line of road

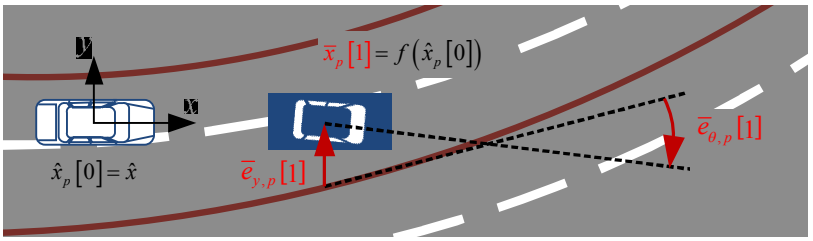

(b) Time-update of Subject Vehicle States and the Relative Error States to Road Geometry

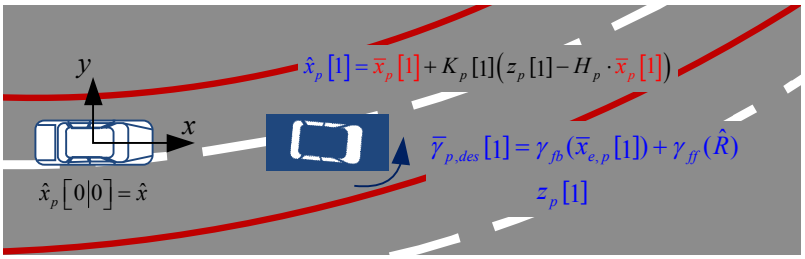

(c) Measurement-update of Subject Vehicle States with Predicted Yaw Rate for Lane Keeping as Virtual Measurement

Figure 2.14. Procedure of State Prediction

2.2.2 Probabilistic Risk Assessment

The potential collision risk between a subject vehicle and surrounding vehicles is represented by the predicted vehicle motions the under the assumptions on their decoupled states. The collision probability is defined as shown in the following equation. The possibility for collision is represented as the surface integral form of the cross product of each probability which means the existence of each vehicle on the pre-defined domain. As the overlapped area of the predicted motion of each vehicle getting large, the probability of collision is also increasing. The probabilistic risk assessment can represent the all-round collision risk of a subject vehicle, and it is available in the various road conditions such as curved road. An existing risk assessment approaches with deterministic behavior only based on current motion such as time-to-collision(TTC) or warning index are hard to represent the actual risk around a subject vehicle on the curved road, because of the omission of the lane information and future behavior of the vehicles around the subject vehicle.

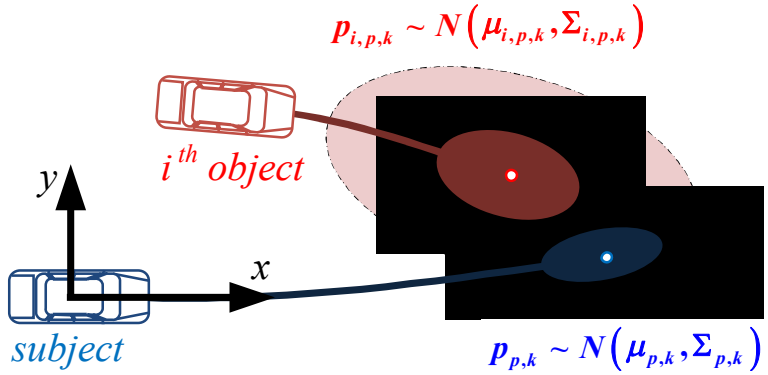

Figure 2.15. Schematic Description of Collision Risk Assessment

$$
\begin{aligned}
&CP_i(k) = \\
&\int_{-\infty}^{\infty}\int_{-\infty}^{\infty}\left\{P\left(X_{i,p,k} \in D_{X_{p,k}}\right)\cdot f_k\left(X_{p,k}\right)\right\} dp_{x,p,k}dp_{y,p,k} \\
&\textit{where,} \\
&P\left(X_{i,p,k} \in D_{X_{p,k}}\right) = \iint_{DX_{p,k}} f_{i,k}\left(X_{i,p,k}\right) dp_{i,x,p,k}dp_{i,y,p,k} \\
&D_{X_{p,k}} = \{(x,y)\,|\,\|x - p_{x,p,k}\| \le \varepsilon_x \cap \|x - p_{y,p,k}\| \le \varepsilon_y\} \\
&X_{p,k} = \begin{bmatrix} p_{x,p,k} & p_{y,p,k} \end{bmatrix}^T
\end{aligned}
\tag{2.20}
$$

Chapter 3

Development of Integrated Safety Control Algorithm

According to the previous research [Althoff 09], the perceptional ability of human drivers is excellent in recognition of an unexpected traffic situation and proper understanding of a traffic situation. Generally, human drivers monitor surrounding environment and predict the future states of surrounding environment based on the current states of that. Then drivers estimate the threat level of possible actions and decide the maneuver of the subject vehicle in consideration of the predicted states of surrounding vehicles during a finite time-horizon. Therefore, in order to develop a highly automated driving system, a safe driving envelope which indicates the drivable boundaries for safe driving over a finite prediction horizon should be determined with the consideration of not only current states of traffic situation surrounding the subject vehicle but also probable future states of that simultaneously [Ferguson 13]. Considering probable future states of surrounding vehicles, it

could be expected that the automated driving control algorithm could handle probable risky situation during a finite time-horizon and enhance safety.

Furthermore, if we define the safe driving envelope based on the probabilistic prediction, it is expected that an automated driving control algorithm which reflects human driver's driving characteristics with an acceptable ride comfort is developed.

3.1 Integrated Risk Representation

In this section, several collision risk representation approaches will be covered. In order to determine the activation level or appropriate intervention timing of advanced driver assistance system such as smart cruise control (SCC), advanced emergency braking (AEB), lane departure warning system (LDWS), lane keeping assistance system (LKAS) or lane change assistance system (LCAS), a various risk indices have been developed so far [Mammar 06, Lee 11]. However, each risk index represents its specific risky scenarios which are longitudinal collision, lane departure, or collision with the vehicle in the blind spot. Since there are many advanced driver assistance modules which can be potentially implemented on the most of the road vehicles, the integration of each risk index is needed.

Recently, several researchers have focused their research on development of new concept of risk index and elaboration of estimation and prediction steps with consideration of uncertainties. For the answer to the first challenge,

Kaempchen et al. defined the collision index by the size of an predicted overlapped area between the host and object vehicle and composed a 2D matrix of collision indices considering all different combinations of possible trajectories of the host and object vehicle [Kaempchen 09]. Some approaches calculate the probability of a collision based on the joint predicted probability density function of the host and the object vehicle [Jansson 04, Lambert 08]. The probability density function is obtained by a Kalman filter, and its

prediction is based on the same simple motion models used in the Kalman filter. As there is no analytical solution to the integral over the joint probability density function, Monte Carlo approximations are performed. For the second demand, the improvement by an integrated particle filter approach is presented by Karlsson et al. [Karlsson 08]. Schubert and Wanielik proposed a direct link between the Bayes filters used by the tracking modules and the situation assessment based on Bayesian networks [Sandblom 11]. Broadhurst et al. presented a prediction and planning framework for analyzing the safety and interaction of moving objects in complex road scenes [Broadhurst 05].

The following section describes the longitudinal and lateral collision risk index, and the newly defined index which is an integrated collision risk index.

3.1.1 Longitudinal and Lateral Collision Risk Indices

In 2007, National Highway Traffic Safety Administration (NHTSA) reported the pre-crash scenario typology for the vehicle safety research in crash avoidance and crashworthiness. The report contains a total of 36 pre-crash scenarios represent 99.4% of all light-vehicle crashes. The total of 36 crash scenarios is classified as a longitudinal collision, lateral collision, baking up collision, control loss, intersection collision and vehicle failure [NHTSA 07].

Table 1. Classification of Pre-Crash Scenario

Crash Type	Frequency [%]	Crash Type	Frequency [%]
Longitudinal Collision	38.95	Control Loss	10.63
Intersection Collision	24.33	Backing up Collision	2.20
Lateral Collision	21.83	Vehicle Failure and Others	2.08

A considerable amount of research has been performed on collision waning systems, which are the first step to assist drivers in collision avoidance. In the view point of preventive safety, deceleration assistance control is effective when collision risk is high and it is difficult for the driver to avoid it. On the other hand, driver can feel anxiety or nuisance against the system if the initiation timing of automatic brake and/or deceleration profile is not

appropriate and it may make the system inefficient. The key is to ensure that control signals are given at the appropriate time, i.e., just in time for drivers to react and avoid collisions while not too early or too frequent to become a nuisance distraction to drivers.

A. Longitudinal Collision Risk Indices

In the prior work, several measures were defined to characterize the emergency level of various dynamic situations, and different sets of human-vehicle experiments were carried out to calibrate these measures to human performances and reactions, based on which different warning criteria were developed to assist drivers [Lee 11]. However, there was no single index good enough to estimate the risk of a rear-end collision because there are various types of traffic situations in the real world. Furthermore, no clear guideline has been established for selecting a suitable index for a given situation.

Thus, in order to develop the acceptable and efficient longitudinal safety system, it is important to select appropriate safety indices and apply them to longitudinal safety system.

This study categorizes the established safety indices as Time relative Indices and Braking relative Indices. Time relative and braking distance relative indices are widely used such as Time To Collision(TTC), and Warning Index(X).

Time to collision (TTC) is defined as the time left to a collision between a

subject vehicle and preceding vehicle assuming that the current relative velocity remains constant. TTC, which is a well-known parameter in longitudinal safety systems, is defined as from the definition with vehicle clearance and velocity:

$$TTC = \frac{c}{v_s} \tag{3.1}$$

TTC is related to the visual cues that might guide driver headway maintenance. The concept of looming, as described in human-factor studies, is employed in the analysis of human perception and longitudinal control behavior in driving situations. The looming effect was first investigated by Hoffman and Mortimer (1996) and was a key factor in the human-centered design of an ACC-with-braking and forward-crash-warning system undertaken by Fancher et al. [Fancher 00]. As illustrated in Figure 3.1, the size of the image that is projected onto the eye of the following driver depends on the range of the observed object, i.e., the preceding vehicle. If there is relative motion between the vehicles, the range, R, and the angle, θ, will change.

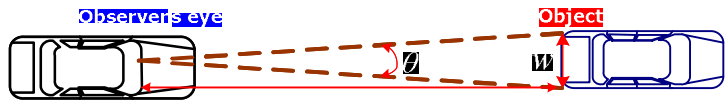

Figure 3.1. Looming Effect of Driver's Eye

The width of the preceding vehicle, w, is constant and can be represented as:

$$w = R \cdot \theta \tag{3.2}$$

The rate of change of the range is related to the rate of change of the angle, θ,

which is occluded by the image as projected onto the observer's eye, i.e., the driver's eye, as follows:

$$\frac{dw}{dt} = 0 = \dot{R} \cdot \theta + R \cdot \dot{\theta} \tag{3.3}$$

The looming effect is represented by the ratio of the occluded angle to the rate of change of that angle, i.e. $\theta / \dot{\theta}$. Therefore, the looming effect can be represented as:

$$\frac{\theta}{\dot{\theta}} = \frac{R}{-\dot{R}} = \frac{c+l}{v_{rel}} \approx TTC \tag{3.4}$$

In Eq. (2.5), l is the distance between the front bumper and the driver's eye. As shown in Eq. (3.2), the driver's sensation of looming is related to the TTC, which is computed using the range and the rate of change of the range.

The non-dimensional warning index represents the danger of physical collision in the current driving situation and is defined as follows:

$$x = \frac{c - d_{br}}{d_w - d_{br}} \tag{3.5}$$

The warning-critical and braking-critical distances are defined as follows:

$$\begin{aligned} d_{br} &= v_{rel} \cdot t_{brake} - \frac{v_{rel}^{\ 2}}{2a_{x,\max}} \\ d_w &= v_{rel} \cdot t_{thinking} + v_{rel} \cdot t_{brake} - \frac{v_{rel}^{\ 2}}{2a_{x,\max}} \end{aligned} \tag{3.6}$$

where, t_{brake} is the system delay, which is given by the brake-system hardware, $a_{\max}$ is the maximum deceleration of the vehicle under driving conditions, $t_{thinking}$ is the delay in human response between recognition and manipulation [Cho 10-2].

These terms can be derived from the kinematics of the two vehicles that

brake to a full stop. If the vehicles start at this distance and brake with their maximum decelerations, they will come to a stop with their bumpers touching each other. To make the critical distance more conservative, two delay terms are added; these account for system and driver delays.

If range exceeds d_{br} and d_w, then the warning index is a positive value that is greater than unity and indicates that the current driving situation is in a safe region. If range is below d_{br}, then the warning index is a negative value and indicates that the current driving situation can be dangerous.

It is shown that the warning index can be influenced by using the maximum deceleration which was able to be obtained from the friction estimation methods as shown in following equations. Each distance is defined with the same way as a longitudinal warning index with respect to an opponent vehicle instead of a subject vehicle. $v_{o,rel}$, v_o and $a_{o,max}$ represent the relative velocity of the vehicles (= v_o-v_s), the velocity and maximum admissible deceleration of the opponent vehicle respectively.

$$d_{br} = v_{o,rel} T_{s,delay} + f(\mu)\left(\frac{v_o^{\,2} - (v_o - v_{rel})^2}{2a_{o,\max}} \right)$$

$$d_w = v_{o,rel} T_{s,delay} + f(\mu)\left(\frac{v_o^{\,2} - (v_o - v_{rel})^2}{2a_{o,\max}} \right) + v_o T_{h,delay} \qquad (3.7)$$

As shown in Figure 3.2, the driving situations can be analyzed in a two-dimensional graph of the warning index vs. the TTC. When the warning index and the TTC is high, the driving situation is in a safe region. However, if the warning index and the TTC gradually decreases, the danger of a rear-end collision increases and the vehicle needs to decelerate to avoid the warning

region. When the warning index and the TTC are low, the driving situation is critical and therefore, the emergency brake should be applied.

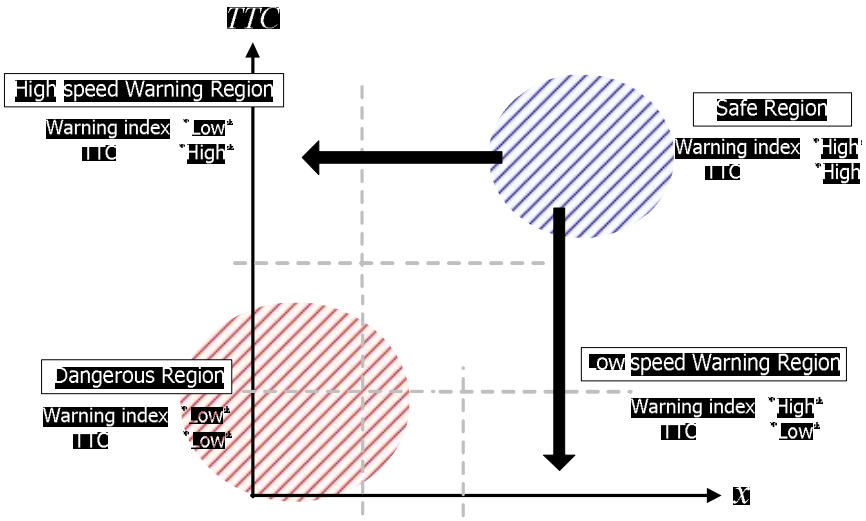

Figure 3.2 Trajectory of the warning index and the inverse TTC for deceleration

A longitudinal index to monitor the vehicle-to-vehicle collision can be determined by using a warning index and an inverse time-to-collision (TTC) which have been developed in previous researches [Moon 08]. In the case of the warning index beyond a threshold value and the inverse TTC below a threshold value, it indicates that the current driving situation is in a safety region. Otherwise, the current driving situation can be dangerous. Therefore the longitudinal index using the warning index and the inverse TTC can be determined as follows:

$$I_{long} = \max\left(\frac{|x_{\max} - x|}{|x_{\max} - x_{th}|}, \frac{|TTC^{-1}|}{|TTC_{th}^{-1}|}\right) \tag{3.8}$$

B. Lateral Collision Risk Indices

According to the recent statistical research of the crash typology in US, A lateral collision caused by lane departure, cut-in and out situation holds 28% of the whole crash typology [NHTSA 07]. In order to reduce the crash caused by lateral collision, a vision sensor attached on the front wind shield has been used for lane departure warning system (LDWS). With the wide application of motor driven power steering (MDPS) system to the commercial vehicle, active safety control for preventing an unwanted lane departure which is lane keeping assistance system (LKAS) has been developed and applied to the commercial vehicle. Furthermore, the vehicle driving in the right behind zone of the subject vehicle can be detected from the rear-side radar and vision. A blind spot detection (BSD) provides acoustic and haptic warning to a driver when a vehicle exists in rear-side of the vehicle [Balcones 09]. The many of the previous researches for preventing lateral collision only use the existence of the rear-side vehicle information or lane information from the rear-side radar and camera. In order to provide more specific information of the rear-side vehicle, high-precision GPS, laser scanner, or vehicle-to-vehicle(V2V) communication are adopted in recent researches, however, the possibility of wide application of those sensors to the commercial vehicle, the high price of the sensors would be a setback.

The representative of the lateral collision warning index is distance to line crossing(DLC) information which can be provided from a front camera. Figure 3.3 shows the schematic description of the lane departure situation.

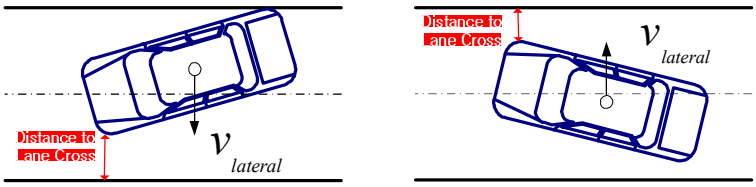

Figure 3.3. Distance to Line Crossing

Time to line crossing can be calculated from the distance to line crossing and the lateral approaching velocity can be estimated as follows:

$$TLC = \frac{DLC}{v_{lateral}} \quad where, v_{lateral} \approx \frac{d(DLC)}{dt} \tag{3.9}$$

The lateral collision risk can be depicted as following figure. A lateral collision can be occurred when a subject vehicle tries to change its lane to the adjacent lane, and the target vehicle in the adjacent lane does not slow down its velocity, v_o, with the clearance between two vehicles, p_{long}.

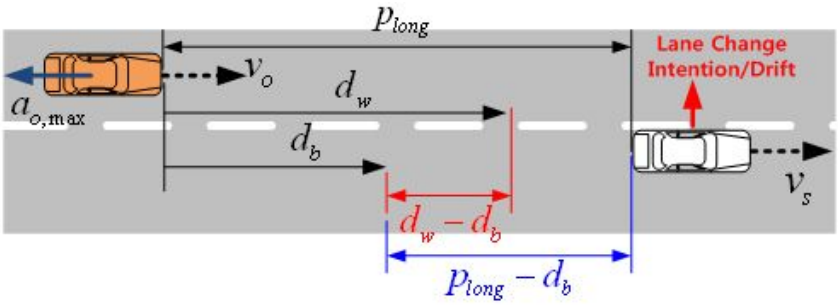

Figure 3.4. Schematic Description of Lateral Collision Risk

Based on the developed longitudinal index and lane information from a front camera, predicted longitudinal collision risk index can be defined. The following figure describes the current position of the subject vehicle and the target vehicle driving in the adjacent lane of the subject vehicle. With the assumption that the subject and target vehicle maintain its current states, the future states of the vehicles can be predicted. A modified longitudinal collision risk index for representing future collision risk can be described as Eq.(3.10).

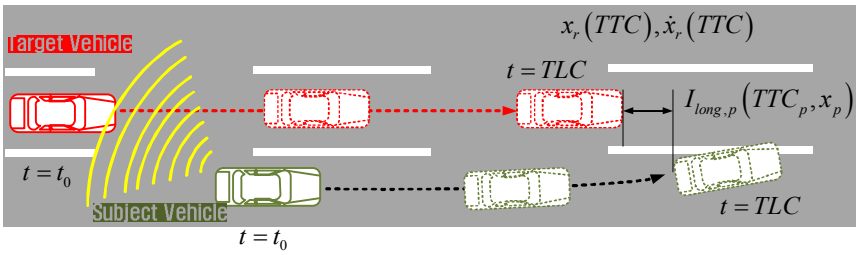

Figure 3.5. Predicted Lateral Collision Scenario

$$I_{long,p}(c + v_{rel} \cdot TLC) = I_{long,p} = \max\left(\frac{|x_{\max} - x_p|}{|x_{\max} - x_{th}|}, \frac{|TTC_p^{-1}|}{|TTC_{th}^{-1}|}\right) \tag{3.10}$$

In order to represent a lateral collision risk within finite time horizon, a lateral collision risk index has been designed using a modified longitudinal collision risk index and time to line crossing as following figure.

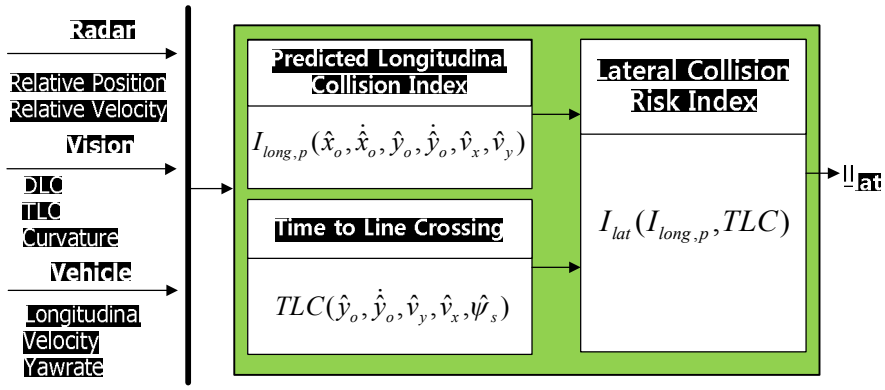

Figure 3.6. Architecture of Lateral Collision Risk Index

A Lateral collision index represents the longitudinal collision risk with the target vehicle behind of a subject vehicle and the lane departure situation simultaneously, and it is limited with the maximum value of 1 as follows:

$$I_{lateral} = \min\left(I_{long,p}, 1\right) \cdot \min\left(\frac{TLC_{th}}{TLC}, 1\right) \tag{3.11}$$

The performance of the lateral collision risk can be verified via simulation. A subject vehicle drives with 110kph and tries to change the lane without noticing a target vehicle driving behind of the subject vehicle as shown in Figure 3.7.

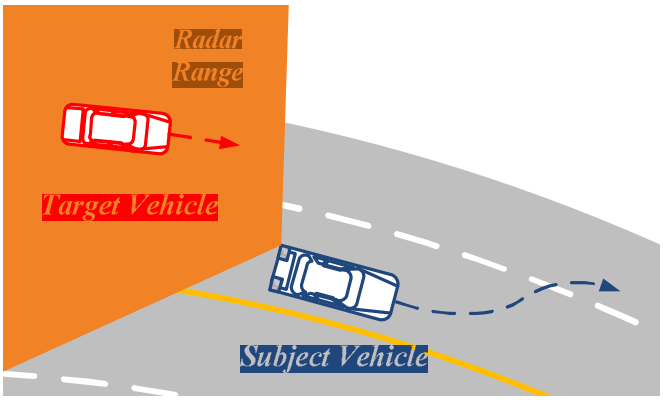

Figure 3.7. Simulation Scenario for Representing Lateral Collision Risk

The longitudinal relative velocity and lateral position of the vehicle are shown in the following results, and the developed lateral collision risk index represents the collision risk described in the scenario as shown in Figure 3.8.

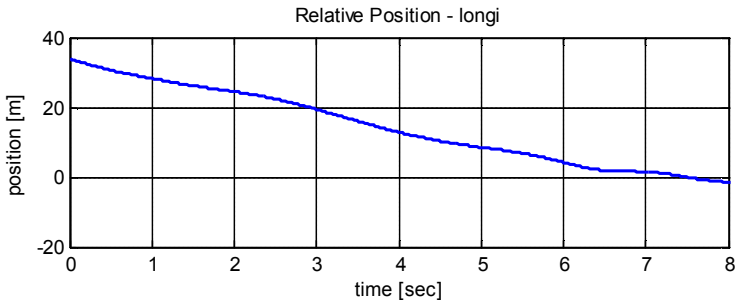

(a) Longitudinal Relative Position

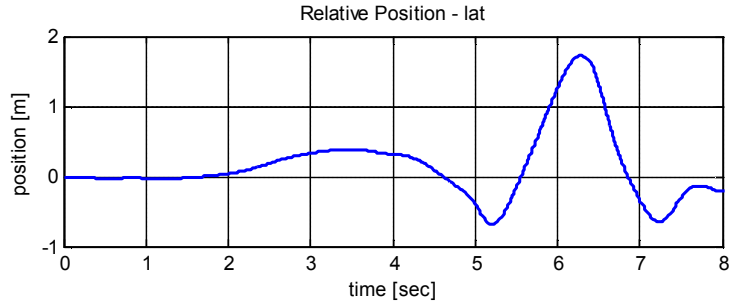

(b) Lateral Relative Position

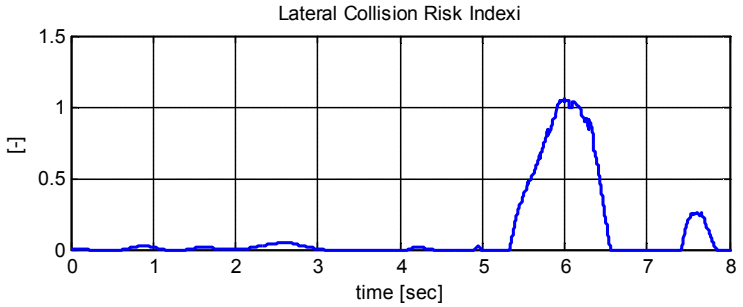

(c) Lateral Collision Risk Index

Figure 3.8. Simulation Results for Lateral Collision Risk Index

3.1.2 Dynamic Drivable Area Determination via Probabilistic Prediction

A. Initial Driving Corridor Decision

An initial driving corridor is determined from detected lanes, rough-precision localization, and digital map stored in advance. The map contains properties of the surroundings potentially helpful for driving, but cannot be reliably detected by sensors such as road width, and global waypoint of center line of total route.

The rough-precision localization is accomplished by combining sensor signals from ego-vehicle chassis and low-cost GPS. The state vector for localization is defined as follows:

$$\mathbf{x} = \begin{bmatrix} p_x & p_y & \psi & v_x & \gamma & a_x \end{bmatrix}^T \tag{3.12}$$

Where, p denotes the relative position, ψ denotes the relative yaw angle, v denotes the velocity, v denotes the yaw rate, and a denotes the acceleration, and subscripts x & y denote x-axis & y-axis of each frame, respectively. The process model is discretized based on no-slip assumption as follows:

$$\begin{aligned} \mathbf{x}[k] &= \mathbf{f}\left(\mathbf{x}[k-1]\right) + \mathbf{w}[k] \\ &= \mathbf{x}[k-1] + \Delta T \cdot \left(\mathbf{a}\left(\mathbf{x}[k-1]\right)\right) + \mathbf{w}[k] \end{aligned} \tag{3.13}$$

$\mathbf{a} = [v_x \cos\psi,\ v_x \sin\psi,\ \gamma,\ a_x,\ 0,\ 0]^{\mathrm{T}}$

$\mathbf{w}[k] \sim (0, \mathbf{W}[k])$

where, **a** is the nonlinear process vector equation, and **w** is the process noise vector being the white noise of covariance **W**. The measurement model for the dead-reckoning is derived as follows:

$$\mathbf{z}_{DR}[k] = \mathbf{h}_{DR}(\mathbf{x}[k]) + \mathbf{v}_{DR}[k]$$

$$\mathbf{h}_{DR,1} = v_x - \frac{w}{2}\cdot\gamma \quad \mathbf{h}_{DR,2} = v_x + \frac{w}{2}\cdot\gamma \quad \mathbf{h}_{DR,5} = \gamma \quad \mathbf{h}_{DR,6} = a_x$$

$$\mathbf{h}_{DR,3} = \begin{pmatrix} \cos\delta\left(v_x - \frac{w}{2}\cdot\gamma\right) \\ +\sin\delta\left(l\cdot\gamma\right) \end{pmatrix} \quad \mathbf{h}_{DR,4} = \begin{pmatrix} \cos\delta\left(v_x + \frac{w}{2}\cdot\gamma\right) \\ +\sin\delta\left(l\cdot\gamma\right) \end{pmatrix} \tag{3.14}$$

$$\mathbf{v}_{DR}[k] \sim \left(0, \mathbf{V}_{DR}[k]\right)$$

Where **h** is the nonlinear measurement vector where the elements are rear-left wheel speed, rear-left wheel speed, front-left wheel speed, front-right wheel speed, yaw rate, and longitudinal acceleration in numeric order. When the GPS is updated, an augmented measurement model is modified as follows:

$$\begin{aligned} \mathbf{z}_{+GPS}[k] &= \mathbf{h}_{+GPS}(\mathbf{x}[k]) + \mathbf{v}_{+GPS}[k] \\ &= \left[\mathbf{h}_{DR}(\mathbf{x}[k]) \quad \mathbf{h}_{+GPS,7} \quad \mathbf{h}_{+GPS,8} \quad \mathbf{h}_{+GPS,9}\right]^T + \mathbf{v}_{+GPS}[k] \end{aligned} \tag{3.15}$$

Where,

$$\mathbf{h}_{+GPS,7} = p_x \quad \mathbf{h}_{+GPS,8} = p_y \quad \mathbf{h}_{+GPS,9} = \psi$$

$$\mathbf{v}_{+GPS}[k] \sim \left(0, \begin{bmatrix} \mathbf{V}_{+DR}[k] & 0 \\ 0 & \mathbf{V}_{+GPS}[k] \end{bmatrix}\right)$$

From the global pose (position and orientation) estimate of the ego vehicle, the nearest segment is selected from the map and transformed to local coordinate. From the detected lane information, distances and angle deviation between the vehicle's pose and the centerline of the local segment are updated with improved accuracy.

It is common practice to describe the forward road geometry by a 2nd-order polynomial. The relation between the ego-vehicle and the road center line can be described by two factors: the relative lateral position and the relative heading angle. With these two factors, the road geometry, which has a curvature radius R, can be approximated by [Schwartz 03]:

$$\begin{aligned} y_r(x) &= \frac{1}{2R}x^2 - \tan e_\theta \cdot x - e_y \\ &= a_2 \cdot x^2 + a_1 \cdot x + a_0 \end{aligned} \tag{3.16}$$

where, x is the down-range distance, and y_r is the lateral position of the corresponding road center in the current body coordinates. As the vehicle drives along its path, the coefficients describing the road geometry vary according to the changing pose of the vehicle on the map. If a state vector is defined as these coefficients, the process model and the measurement model can be derived as follows:

$$
\begin{aligned}
\dot{\mathbf{x}}_{\mathbf{r}} &= \mathbf{A}_{\mathbf{r}}\mathbf{x}_{\mathbf{r}} + \mathbf{B}_{\mathbf{r}}\mathbf{u}_{\mathbf{r}} + \mathbf{w}_{\mathbf{r}} \\
&= \begin{bmatrix} 0 & 0 & 0 \\ 2v_x & 0 & 0 \\ 0 & v_x & 0 \end{bmatrix} \begin{bmatrix} a_2 \\ a_1 \\ a_0 \end{bmatrix} + \begin{bmatrix} 0 \\ -1 \\ 0 \end{bmatrix} \gamma + \mathbf{w}_{\mathbf{r}} \qquad (3.17) \\
\mathbf{w}_{\mathbf{r}} &\sim \left(\mathbf{0} \quad \mathbf{Q}_{\mathbf{r}}\right) \\
\mathbf{z}_{\mathbf{r}}[k] &= \mathbf{H}_{\mathbf{r}}\mathbf{x}_{\mathbf{r}}[k] + \mathbf{v}_{\mathbf{r}}[k] \\
&= \begin{bmatrix} 1 & 0 & 0 \\ 0 & 1 & 0 \\ 0 & 0 & 1 \end{bmatrix} \mathbf{x}_{\mathbf{r}}[k] + \mathbf{v}_{\mathbf{r}}[k] \\
\mathbf{v}_{\mathbf{r}}[k] &\sim \left(\mathbf{0} \quad \mathbf{V}_{\mathbf{r}}\right)
\end{aligned}
$$

Where, the subscript *r* is used to denote relation to the road geometry states. The Kalman filter is used for the estimation of road geometry coefficients. The best estimate result of the localization is used for the longitudinal velocity and the yaw rate. Hence, the covariance of the process noise should be well defined so that it can represent the effect of the estimate error of the vehicle motion filtering. As the result, the estimate of the initial driving corridor coefficients is recursively estimated using the Kalman filter [Re 60]. Both detected lane marker and selected local segment are used for measurement update. Note that the covariance of the measurement noise should represent both localization error and lane detection error.

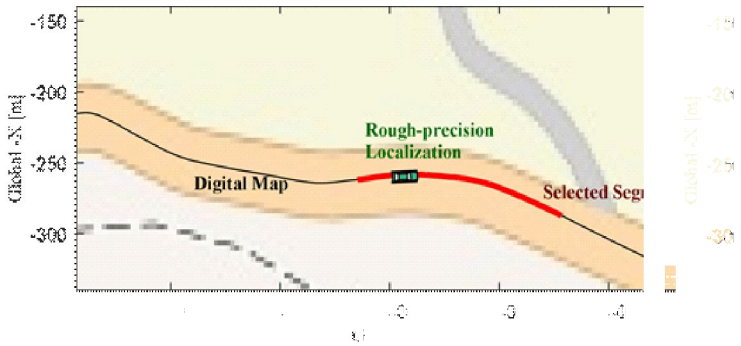

(a) Nearest segment selection

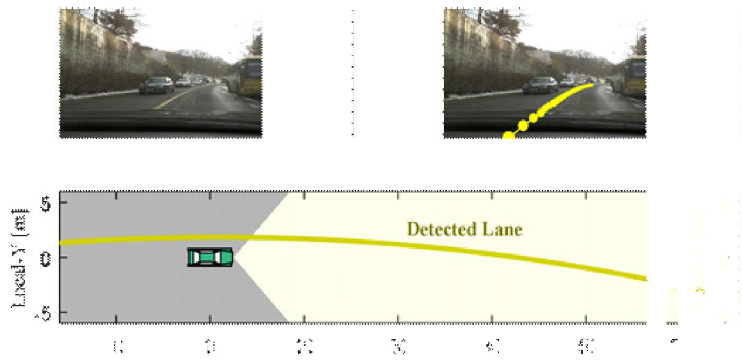

(b) Lane detection

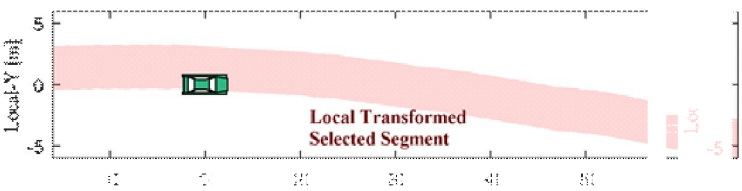

(c) Segment transformation to local coordinate

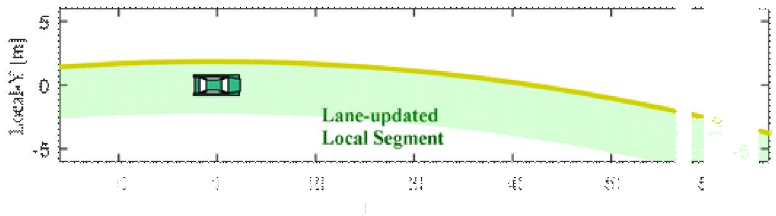

(d) Lane-level segment matching

Figure 3.9. Sequences of initial driving corridor decision.

Figure 3.9 shows an example of sequence of initial driving corridor decision. Figure 3.9(a) shows a nearest segment selection from the map data. Digital map is depicted as black line, rough-precision global pose estimate result is depicted as green vehicle, and the selected nearest segment is depicted as the thick-red line. Figure 3.9(b) shows a lane detection result; the yellow centerline. Figure 3.9(c) shows a segment transformed to local coordinate. Due to the error in the global pose estimate, the ego-vehicle seems deviated from the lane (actually not). Figure 3.9(d) shows lane-level segment matching result. By matching the locally transformed segment with the detected lane marker, the updated local segment is now more accurate.

B. Moving Object Tracking and Prediction

One important factor in autonomous driving in rural roads is all-around

monitoring for other traffics. One long-range radar (front) and a set of three mid-range radars (front, rear-left, and rear-right) were selected to fulfil this perception task.

Reliably detecting and tracking other traffics such as preceding and oncoming vehicles is one of the most important tasks. And another essential task is to estimate and predict the target vehicles' overall states such as heading, yaw rate, absolute velocity and acceleration as well as relative position and relative velocity.

To achieve these tasks, an interacting multiple model approach using extended Kalman filters (EKF) was employed to improve multi-target states estimation performance [Furgale 13].

Various driving patterns of a vehicle including straight line, curve, cut-in/out, U-turn and interchange can be represented by a combination of a constant velocity rectilinear motion, a constant acceleration rectilinear motion, a constant angular velocity curvilinear motion and a constant angular acceleration curvilinear motion. To describe all these motions, the state vector and input vector of target *n* are defined as follows:

$$\mathbf{x}_n = \begin{bmatrix} p_{n,x} & p_{n,y} & \theta_n & v_{n,x} & \gamma_n & a_{n,x} & \dot{\gamma}_n \end{bmatrix}^T \tag{3.18}$$

$$\mathbf{u} = \begin{bmatrix} v_x & \gamma \end{bmatrix}^T$$

Where, subscripts x and y denote x-axis and y-axis of each frame, subscript n denotes "of target n", p denotes the relative position θ denotes the relative yaw angle, v denotes the velocity, γ denotes the yaw rate, a denotes the acceleration, and $\dot{\gamma}$ denotes the yaw acceleration. And variable without subscript n means "variable of the host vehicle". Therefore v_x denotes the longitudinal velocity of host vehicle and γ denotes the yaw rate of host vehicle. Note that $p_{n,x}$, $p_{n,y}$ and θ_n are defined on the host vehicle's body-fixed moving frame, {1}, and other elements are defined on the ground-based fixed frame, {0}.

In an automotive target tracking, changes in the target aspect with respect to the radar can cause the apparent point of radar reflections (relative position seen by the antenna) to wander significantly. To represent these characteristics, the measurement model can be elaborated by introducing new parameters to specify the sensor position and the measured point as shown in Figure 3.10. As the result, $z_n[k]$, the measurement vector of target n is defined as follows.

$$\begin{aligned}\mathbf{z}_n[k] &= \mathbf{h}\left(\mathbf{x}_n[k], \mathbf{u}[k]\right) + \mathbf{v}_n[k] \\ &= \begin{bmatrix}\mathbf{h}_{n1} & \mathbf{h}_{n2} & \mathbf{h}_{n3}\end{bmatrix}^T + \mathbf{v}_n[k] \\ \mathbf{v}_n[k] &\sim \left(0, \mathbf{V}_n[k]\right)\end{aligned} \tag{3.19}$$

where,

$$\mathbf{h}_{n1} = p_{n,x} - s_x + b_{n,x}\cos\theta_n - b_{n,y}\sin\theta_n$$
$$\mathbf{h}_{n2} = p_{n,y} - s_y + b_{n,x}\sin\theta_n + b_{n,y}\cos\theta_n$$
$$\mathbf{h}_{n3} = v_{n,x}\cos\theta_n - v_x + p_{n,y}\cdot\gamma + \left(b_{n,x}\sin\theta_n + b_{n,y}\cos\theta_n\right)\left(\gamma - \gamma_n\right)$$

Where, **h** is nonlinear measurement equation describing the state of measured point on the sensor based moving frame {2}. *s* is sensor position vector defined on the host vehicle's body-fixed moving frame {1} and b_n is measured point vector of target *n* defined on the target vehicle's body-fixed moving frame {3}. The first order approximation of the measurement error covariance has been presented in previous works as follows:

$$\mathbf{V}_n = \begin{bmatrix} \dfrac{\sigma_r^2 - r_n^2\sigma_\theta^2}{2}\begin{bmatrix} b_n + \cos 2\theta_n & \sin 2\theta_n \\ \sin 2\theta_n & b_n - \cos 2\theta_n \end{bmatrix} & \mathbf{0}_{2\times 1} \\ \mathbf{0}_{1\times 2} & \sigma_v^2 \end{bmatrix} \tag{3.20}$$

where,

$$b_n = \frac{\sigma_r^2 + r_n^2\sigma_\theta^2}{\sigma_r^2 - r_n^2\sigma_\theta^2} \quad r_n = \sqrt{\mathbf{h}_{n1}^2 + \mathbf{h}_{n2}^2} \quad \theta_n = \tan^{-1}\left(\frac{\mathbf{h}_{n2}}{\mathbf{h}_{n1}}\right)$$

where, γ_n and θ_n are the range and azimuth measurements, respectively. σ_r, σ_θ and σ_v are the standard deviations of the range, the azimuth and the relative velocity, respectively. The approximation is validated to be useful for practical parameters. The various measurement patterns due to the target aspect with respect to radar can be represented by the above standard measurement model by adjusting the measured point vector $\boldsymbol{b}_n$. A detailed description of the IMM/EKF based multi-target tracing algorithm can be found in [Schwartz 03].

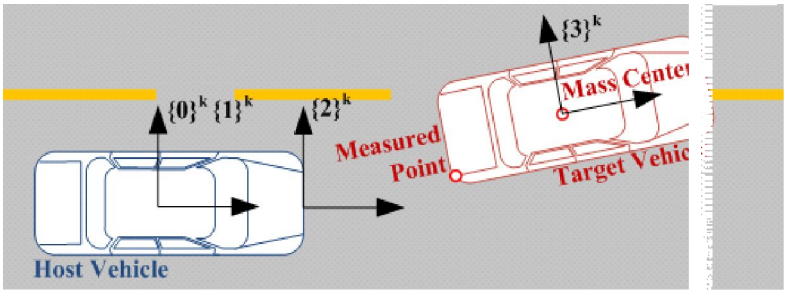

(a) at time k

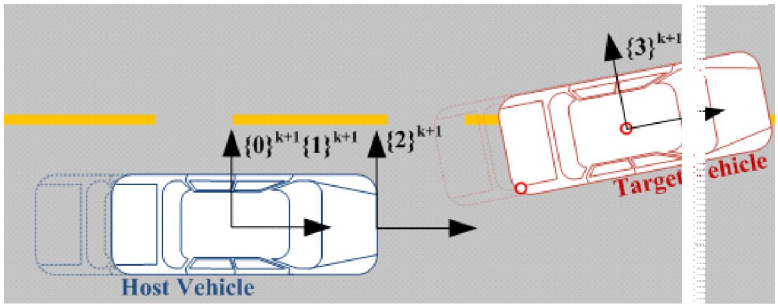

(b) at time k+1

Figure 3.10. Four coordinate systems used to derive standard process model and standard measurement models.

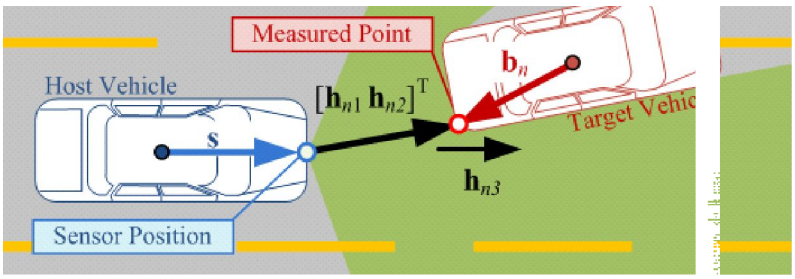

Figure 3.11. Parameters to derive the standard form of the refined measurement model.

The possible behaviors of surrounding vehicles are predicted and considered in determining the safe drivable area decision. To predict reasonable ranges of the future states of surrounding vehicles, driving data is collected on test tracks and real roads and analyzed the probabilistic movement characteristics of the vehicle.

The future vehicle states are described as a stochastic multi-stage process via Taylor Method. At every time step of the prediction time horizon, a desired yaw rate is determined by the lane-keeping driver model. Assuming that the measurement noise has a normal distribution with zero mean, the predictive measurement is linearly related to the time-updated predictive state. Then, the maximum likelihood prediction of the future state is calculated by the Kalman filtering equations.

C. Dynamic Drivable Area Decision

The safety envelope decision module determines the complete driving corridor that leads to the destination while assigning all objects to either the left or right corridor bound. In the case of moving objects such as other traffic participants, their behaviours are anticipated within a finite time horizon.

Dynamic drivable area which is a safety envelope decision process is as

follows. The safety envelope decision module first starts with an initial driving corridor from a prior road information map. The module asserts whether the ego-vehicle stays in the bounds of this corridor. On top of this initial driving corridor, static obstacles represented on the occupancy grid map are combined; hence, either the left or right corridor bound would be "eroded" by the static obstacle. To determine which side of the bounds a static obstacle would "erode", for each obstacles grid, decision on whether its left or right side should the ego-vehicle pass is made. After having assigned all obstacle grids to either side of the corridor bound, geometric constraints for motion optimization are newly computed considering e.g., driver acceptance, sensor uncertainty, and control uncertainty.

To accommodate moving vehicles within a finite time-horizon, their future states are considered probabilistically. To achieve this, as described in 0, every moving vehicle detected by the sensor system is associated with one lane and its future motion is predicted in probabilistic methodology, assuming that the vehicle follows the lane with acceptable deviation. Similar to the static obstacles, safety envelop boundaries are eroded be each prediction result. However, because the object is in motion, each envelop erosion is active for a specific time step only.

Therefore, the relative complement of predicted areas of moving objects

and unsafe regions due to static obstacles in the initial driving corridor is the set of drivable area at each time step, also termed “safety driving envelope”.

Figure 3.12 depicts the safety envelop decision results when there are several parallel parked buses on the right side as static obstacles and an oncoming vehicle on the left lane as one moving obstacle. All variables are expressed in terms of the current local coordinate of ego vehicle. Here, the initial driving corridor is shown as green area, newly computed geometric constraints due to static obstacle as red area, and active constraints due to the moving object at each time step as blue area. The blue vehicle and the green vehicle indicate the predicted oncoming vehicle and the predicted ego-vehicle, respectively. It is notable that the active constraint due to moving object is enlarged as longer T_p, the prediction interval, is used. The safety driving envelope can be defined as the relative complement of blue and red area in green area, at each time step.

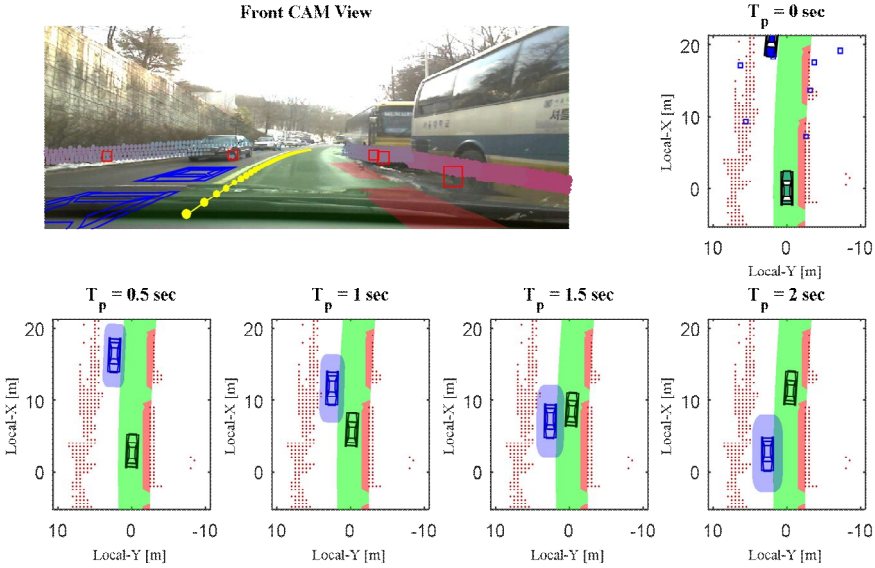

Figure 3.12. Safety envelop decision results at different time steps.

3.2 Desired Motion Determination for Safety Control

This section describes the desired motion determination for collision avoidance and lane guidance. An artificial potential field approach has been considered to represent the potential risk of surrounding vehicles. A motion control based on predicted motion of a host vehicle and around vehicle and its predicted potential risk has been developed within a dynamic driving envelope. In order to guarantee the safety driving, the dynamic driving envelope has been set to be a boundary of the controlled motion. Yaw rate candidates and longitudinal acceleration candidates are developed within the dynamic driving envelope, considering the stability constraints of the vehicle which should be guaranteed for the lateral stability. Each desired motion candidate are propagated within the future time horizon, and the desired motion at each time step is selected from the predefined performance function minimizing the magnitude of the control input, the rate of change of the control input and predicted potential risk function around the subject vehicle.

3.2.1 Potential Field Representation

Typical path planning using potential field consists of two different types of energy functions which are an attractive potential and repulsive potential. The attractive potential generates the attractive force between the subject and the pre-defined goal point. The repulsive potential generates the force which prevents the subject to get close to the obstacles and keeps the marginal distance. The first step of the potential field approach is calculating the gradient of the summation of each pre-defined potential energy function which is a resultant force as follows:

$$F_{result} = -\nabla\left(U_a(q) + U_r(q)\right) \tag{3.21}$$

The following step is to find the desired path based on the resultant force. A gradient descent algorithm is the most popular method which has been widely used for path planning using a potential field approach as:

$$q_{i+1} = q_i + f\left(F_{result}(q_i)\right) \tag{3.22}$$

The function of resultant force is usually represented as the production of unit vector of the resultant force and a fixed step size. This kind of approach may cause a local minimum problem which makes the calculated path remain around the local solution of the path, not a global goal point. In order to deal with this kind of local minimum problem, various approaches have been developed so far [Liu 00].

For an automated vehicle, which has pre-defined way points using GPS/INS, the potential field approach can be adopted to find the path for

avoiding collision with local obstacle by the desired motion from repulsive potential. Furthermore, in order to guarantee the real time performance of the motion planning, the algorithm should be confirmed with computational efficiency.

The risk potential in driving situation can be represented as following figure. The collision risks are assessed by predicted motion of the surrounding vehicles in various driving conditions.

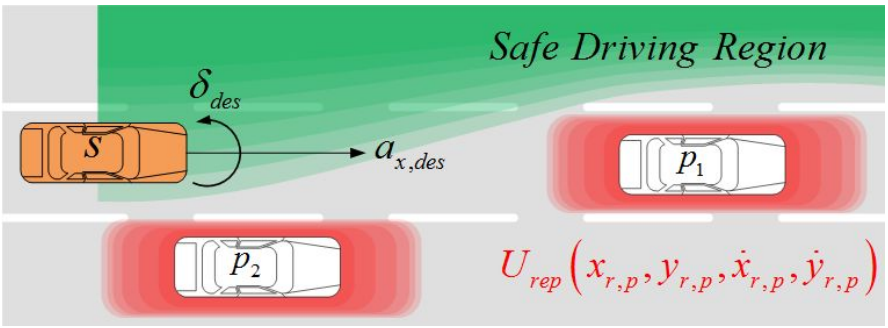

Figure 3.13. Schematic Description of Risk Potential to Surround Vehicles

In order to determine the desired motion for collision avoidance, the repulsive potential energy function has been designed as follows:

$$U_{rep} = \begin{cases} k \cdot f\left(CP_i\right) \cdot \exp\left(-\left(\dfrac{x_{r,p}}{\dot{x}_{r,p}}\right)^2 - \dfrac{y_{r,p}^2}{w_y^2}\right) & if \ \left\|\rho\left(x_{r,p}, y_{r,p}\right)\right\| \le \rho_{long} \\ 0 & else \end{cases} \tag{3.23}$$

where, $x/y_{r,p}$ and $\dot{x}/\dot{y}_{r,p}$ denote the longitudinal/lateral distance between the subject vehicle and target vehicle, and relative longitudinal/lateral velocity, respectively. k represents the stiffness of the repulsive energy. $f(CP_i)$ denotes

the i-th normalized collision probability representing the normalized probability between 0 to 1. The magnitude of the risk potential increases when the subject vehicle approaches the obstacle near the safety margin, or the subject vehicle is getting closer to the obstacle with high relative speed.

3.2.2 Vehicle Motion Control based on Predictive Risk Potential Energy Function

The desired motions for automated driving control are determined with longitudinal / lateral candidate motions as shown in the Figure 3.14. The boundaries of the candidate motion are determined from the collision risks around the subject vehicle, i.e., the vehicles in left-lane, right-lane and in-lane. The candidate motions for longitudinal and lateral safety are discretized within the predicted time horizon [Takahiro 14].

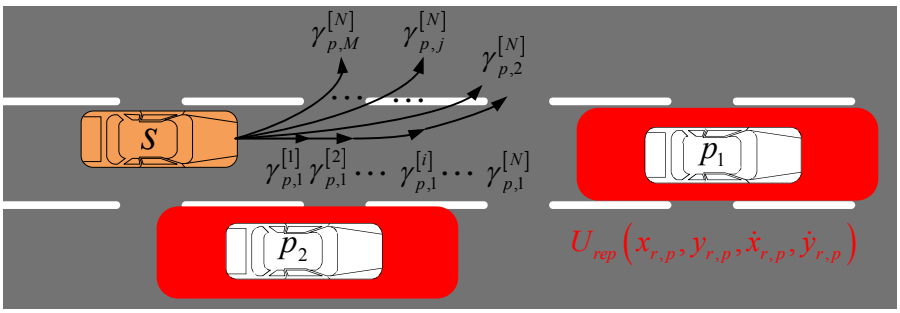

(a) Desired Yawrate Candidates for Lateral Safety Control

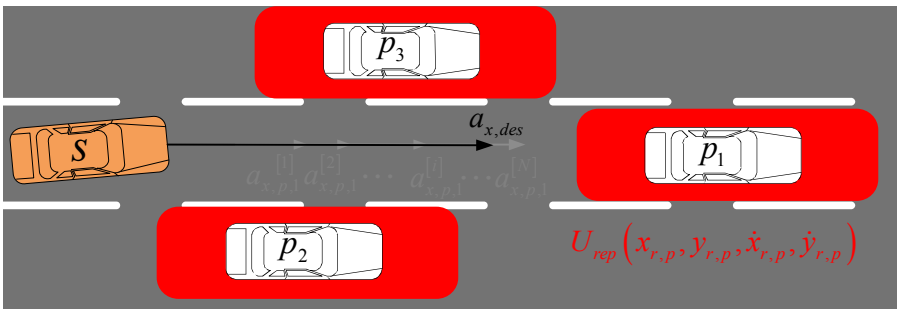

(b) Desired Acceleration Candidates for Longitudinal Safety Control

Figure 3.14. Desired Motion Candidates for Lateral and Longitudinal Control

In order to consider the future risk potential according to the future controlled motion from yaw rate candidates, coordinate transformation is needed from the motion prediction based on the current driving status. The states of the vehicles are defined as follows:

$$\underline{x}_{rel}(i) = \left[I_{on}(i) \quad p_{x,rel}(i) \quad p_{y,rel}(i) \quad v_{x,rel}(i) \quad v_{y,rel}(i) \quad CP(i) \right]^T \tag{3.24}$$

With the controlled yaw motion from the yaw rate candidates, the predicted position of controlled vehicle can be transformed as following equation.

$$\begin{aligned} &for\ \gamma_j \\ &\quad x(k+1) = x(k) + v_x(k) \cdot \cos\psi(k) \cdot \Delta t \\ &\quad y(k+1) = y(k) + v_x(k) \cdot \sin\psi(k) \cdot \Delta t \\ &\quad \psi(k+1) = \psi(k) + \gamma_j \cdot \Delta t \\ &end \end{aligned} \tag{3.25}$$

Figure 3.15 shows the predicted motion of controlled vehicle by the specific yaw rate. If there are a preceding vehicle to be taken over, and the other vehicle driving in the left lane of the subject vehicle, the subject vehicle tries to change its lane to the right side. In this lane change situation with steering control input, the predicted potential risk energy function can be calculated based on the transformed future motion of the subject and surround vehicle. $U_{rep}(i)$ denotes the predicted risk potential energy function of the i-th time step within the finite time horizon.

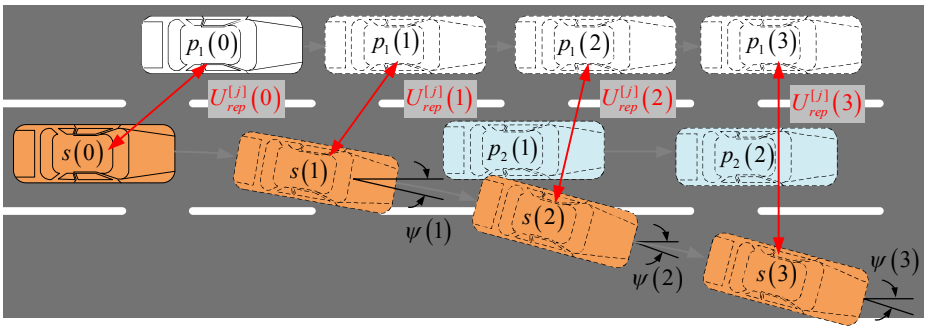

Figure 3.15. Predicted Potential Energy Function

Cost functions for the desired longitudinal and lateral motion are defined with the potential energy function of predicted motions of the subject and object vehicles, and control input limitations such as the norm of control input, and the rate of control input as shown in Figure 3.15. The desired motions can be determined from the pre-defined cost functions to be minimized within control input boundaries.

$$J_{lat}(j) = \sum_{i=1}^{N} \begin{pmatrix} w_1 \cdot U_{rep}\left(x_{r,p}(j), y_{r,p}(j), \dot{x}_{r,p}(j), \dot{y}_{r,p}(j)\right) \\ + w_{lat,1} \cdot \left(\gamma_{p,j}^{[i]}\right)^2 \end{pmatrix} + w_{lat,2} \sum_{i=0}^{N-2} \left(\gamma_{p,j}^{[i+1]} - \gamma_{p,j}^{[i+1]}\right)^2 \tag{3.26}$$

$$J_{long}(j) = \sum_{i=1}^{N} \begin{pmatrix} w_1 \cdot \left(U_{rep}\left(x_{r,p}(j), y_{r,p}(j), \dot{x}_{r,p}(j), \dot{y}_{r,p}(j)\right)\right) \\ + w_{long,1} \cdot \left(a_{x,p,j}^{[i]}\right)^2 \end{pmatrix} + w_{long,2} \sum_{i=0}^{N-2} \left(a_{x,p,j}^{[i+1]} - a_{x,p,j}^{[i]}\right)^2$$

$$u_{k,des} = \underset{u_{k,\min} \le u_k \le u_{k,\max}}{\arg\min} \left(J_k(j)\right), \; k \in [long \; lat]$$

A potential field approach can be applied for lane keeping situation

[Rossetter 05]. The previous research proposed a potential energy function including the heading angle of the vehicle to the lane, which is provided a vision sensor with low reliability. A proposed risk potential includes the relative distance and velocity to the center lane which can be calculated with the measured lane information from vision sensor such as distance-to-line crossing(DLC) and time-to-line crossing(TLC) represented as:

$$\hat{v}_y = v_x \cdot \psi \approx \frac{d(DLC)}{dt} \tag{3.27}$$

$$TLC = \frac{DLC}{\hat{v}_y}$$

The artificial risk potential is assessed around the center lane as shown in Figure 3.16 with the same concept of safety margin represented as Eq. (3.28).

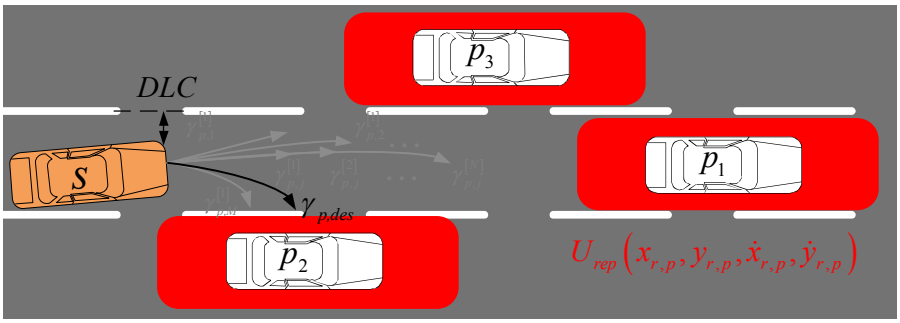

Figure 3.16. Description of Lane Departure Situation

$$J_{lane}(j) = \sum_{i=1}^{N}\left(w_1 \cdot U_{rep,lane}\left(DLC, \psi_{heading}\right) + w_{lane,1} \cdot \left(\gamma_{p,j}^{[i]}\right)^2\right) + w_{lane,2}\sum_{i=0}^{N-2}\left(u_{lat}^{[i+1]} - u_{lat}^{[i]}\right)^2 \tag{3.28}$$

$$\gamma_{des} = \underset{u_{\min} \le \gamma \le u_{\max}}{\arg\min}\left(J_{lane}(j)\right)$$

A driving mode of automated driving is determined as the following

procedure represented in Figure 3.17. A subject vehicle drives with pre-defined set speed with lane keeping control in the low collision risk situation with front vehicle. If the collision risk of the front vehicle increases, the control algorithm should determine the driving mode for collision avoidance with lane change or lane keeping with speed control under the consideration of the collision risks of the vehicle in left land and right lane.

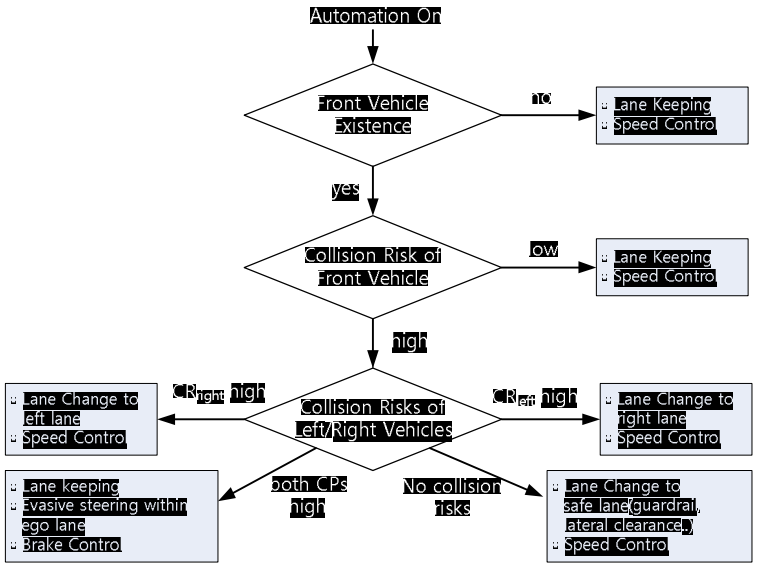

Figure 3.17. Driving Mode Decision Procedure

3.2.3 Dynamic Constraints

The boundary of the controlled motion is determined from a dynamic drivable area which is safety driving envelope. However, within the safety driving envelope, longitudinal and lateral constraints coming from a vehicle dynamics should be considered to guarantee the stability, and actuator limitations.

Several constraints between the vehicle and ground are considered to ensure vehicle dynamic stability along the path. The constraints treated in this section include: 1) limits on tire force, and limits on the lateral motion which includes 2) limits on steering characteristics, 3) limits on side slip behavior, and 4) limits on rollover characteristics. Each longitudinal and lateral motion of the vehicle should be bounded with the physical constraint and dynamic constraint corresponding with the vehicle speed.

A. Dynamic Constraints of Longitudinal Dynamics

The braking pressure produces the friction force tangent to the path at the contact patch. Normally the friction force is proportional to the measured brake pressure. The friction force is represented with the normal load on the tire, the friction coefficient of the tire-road interface, and the slip ratio defined as follows:

$$\lambda = \frac{r_{eff}\omega_w - v_x}{v_x},\ during\ braking$$
$$\lambda = \frac{r_{eff}\omega_w - v_x}{r_{eff}\omega_w},\ during\ acceleration \qquad (3.29)$$
$$where,\ r_{eff} = effective\ radius\ of\ the\ tire$$
$$\omega_w = rotational\ velocity\ of\ the\ wheel$$

When the longitudinal slip ratio is small(less than 0.1 on dry asphalt), the friction force is found to be proportional to the slip ratio with longitudinal tire stiffness as shown in Figure 3.18.

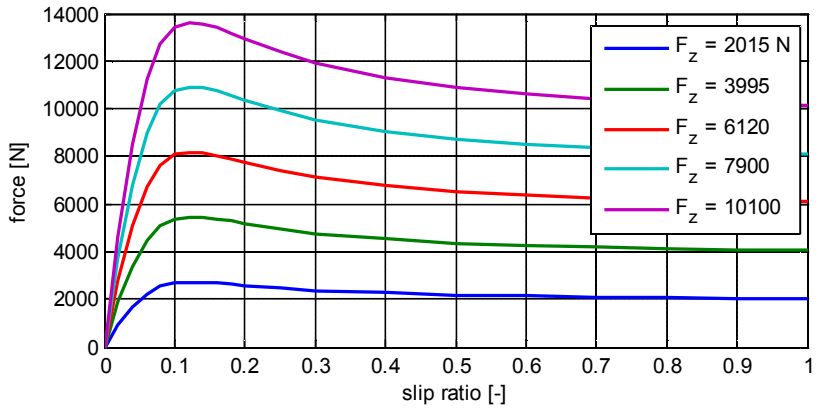

Figure 3.18. Longitudinal Tire Force Characteristics

The maximum tire friction force for passenger cars can be determined tire characteristics, and the driving force is directly related with the maximum engine force. These limitations are assumed to be constant and independent of speed. The following equation yields the feasible deceleration range due to constraints on the tire friction force.

$$-\frac{F_{x,\max}}{m} \le a \le F_{engine} \tag{3.30}$$

B. Dynamic Constraints for lateral stability

Limits on the lateral motion of the vehicle are represented with the steering constraint, side slip constraint, and rollover constraint. The states within the area denote the stable condition in the current driving situation, and the boundary around the area represents the marginal states guaranteeing the stable condition. The following equation represents the relationship between the lateral acceleration, yaw rate and longitudinal velocity in steady-state case [Matthew 06].

$$a_y = \dot{v}_y + v_x \cdot \gamma \approx v_x \cdot \gamma \tag{3.31}$$

A steering constraint represents the limitation on the lateral acceleration by maximum steering angle attainable with dynamic handling properties of a vehicle. The dynamic handling properties are obtained from a 2-DOF bicycle model represented as:

$$\begin{aligned} m \cdot a_y &= 2C_f \cdot \alpha_f \cdot \cos\delta_f + 2C_r \cdot \alpha_r \\ I_z \cdot \dot{\gamma} &= 2l_f \cdot C_f \cdot \alpha_f \cdot \cos\delta_f - 2l_r \cdot C_r \cdot \alpha_r \approx 0 \end{aligned} \tag{3.32}$$

Where, α_f and α_r represent the wheel slip angle at front and rear wheel.

From the definition of the slip angle, the following relationship can be derived with the understeer gradient K_{steer}:

$$\delta_f = K_{steer} \cdot a_y + \left(l_f + l_r\right)\frac{\gamma}{v_x}$$
$$K_{steer} = \frac{m \cdot l_r}{2C_f \cdot \left(l_f + l_r\right) \cdot \cos\delta_f} - \frac{m \cdot l_f}{2C_r \cdot \left(l_f + l_r\right)} \tag{3.33}$$

From the above equations, the steering constraint in the current states is represented with the maximum steering angle, which is near 540deg in a passenger car, current front steering angle, and vehicle speed.

$$\left|\gamma\right| \le \frac{\delta_{\max} \cdot v_x}{Ksteer \cdot v_x^2 + \left(l_f + l_r\right)} \tag{3.34}$$

Figure 3.19 presents the drivable area considering with the steering constraint. A blue line represents the marginal yaw rate according to the vehicle driving speed. A vehicle can generate the maximum yaw rate without any slip with its maximum steering input on the blue line of the figure.

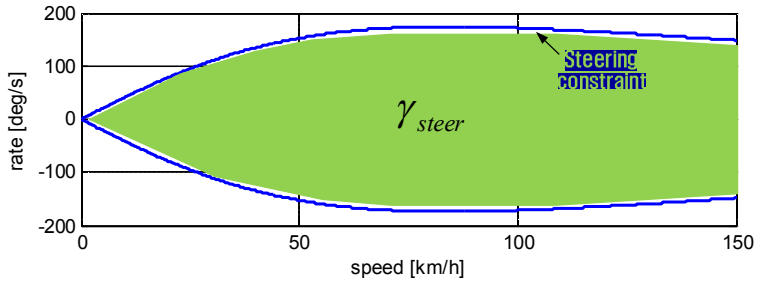

Figure 3.19. Dynamic Drivable Area within Steering Constraint

A side slip constraint represents the maximum yaw rate of a vehicle within the boundary of lateral stability. A vehicle shows the skid maneuvering when a magnitude of the lateral force exceeds the physical limit of tire-road friction.

The slip constraint is derived from the tire-road friction including road friction coefficient, μ, as following equation:

$$m \cdot |a_y| \le \mu \cdot m \cdot g \tag{3.35}$$

A side slip constraint is represented with the tire-road friction and current speed of a vehicle.

$$|\gamma| \le \frac{\mu \cdot g}{v_x} \tag{3.36}$$

Figure 3.20 represents the drivable area satisfying both steering constraint and side slip constraint. It guarantees its lateral stability without any slip motion of a vehicle. A steering constraint represented in blue line in the figure shows more tighter condition in a low speed under 30kph than the side slip constraint, which means even with the maximum steering angle, the vehicle cannot be unstable in lateral direction.

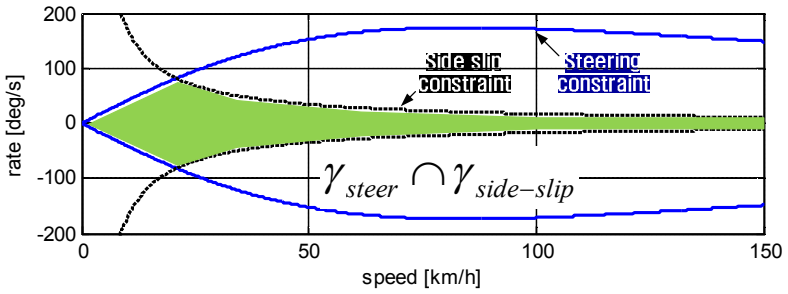

Figure 3.20. Steering and Side Slip Constraints

A rollover constraint which represents the limit of lateral acceleration for rollover prevention can be obtained from rollover index [Yoon 07]. A rollover

risk can be determined with the following factors: 1) roll angle and roll rate, 2) lateral acceleration, and 3) time to wheel lift of a vehicle. The rollover index(RI) is calculated by using the lateral acceleration which can be measured from electronic stability control(ESC) module, the estimated roll angle, the estimated roll rate, and their critical values as follows:

$$RI = \begin{cases} C_1 \dfrac{|\phi(t)|\cdot\dot{\phi}_{th} + |\dot{\phi}(t)|\cdot\phi_{th}}{\phi_{th}\cdot\dot{\phi}_{th}} + C_2\dfrac{|a_y|}{a_{yc}} + C_3\dfrac{|\phi(t)|}{\sqrt{\phi(t)^2+\dot{\phi}(t)^2}}, & K_r > 0 \\ 0 \quad , K_r \le 0 \end{cases} \tag{3.37}$$

$$where,\ K_r = \phi\cdot\left(\dot{\phi} - k_1\phi\right)$$

where, $C_1+C_2+C_3=1$. C_1, C_2, C_3 and k_1 are positive constants. The subscript th represents the critical value of each state. The maximum lateral acceleration which keeps the rollover index below the critical value can be represented as follows:

$$a_{y,roll,\max} = \frac{a_{y,c}}{C_2}\left(RI_{tar} - C_3\cdot\frac{|\phi(t)|}{\sqrt{\phi(t)^2+\dot{\phi}(t)^2}} - C_1\cdot\frac{|\phi(t)|\dot{\phi}_{th} + |\dot{\phi}(t)|\phi_{th}}{\phi_{th}\dot{\phi}_{th}}\right) \tag{3.38}$$

$$where,\ RI_{tar} = Target\ \ Rollover\ \ Index$$
$$a_{y,c} = Critical\ \ Acceleration$$

RI_{max} denotes the maximum rollover index. The maximum yaw rate considering rollover prevention can be represented as follows:

$$|\gamma| \le \frac{a_{y,roll,\max}}{v_x} \tag{3.39}$$

A steering constraint, side slip, and rollover constraints are subspaces of the drivable area, which included the set of vehicle longitudinal speed and yaw rate which are attainable at a given instant as shown in following figure.

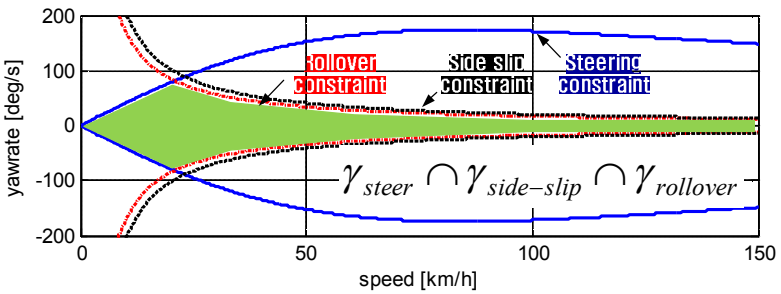

Figure 3.21. Final Drivable Area for Lateral Stability

The desired motions for collision avoidance derived by the risk potential function should be bounded within the drivable area. In consequence, the desired motions can be represented as follows:

$$a_{y,des} = \begin{cases} a_{y,\max} & if\ a_{y,des} > a_{y,\max} \\ \dfrac{F_r}{m} & if\ a_{y,\min} < a_{y,des} < a_{y,\max} \\ a_{y,\min} & if\ a_{y,des} < a_{y,\min} \end{cases} \tag{3.40}$$

The desired steering wheel angle can be obtained by desired lateral acceleration considering the dynamic constraints as following equation.

$$\delta_{des} = a_{y,des}\left(\frac{l_f + l_r}{v_x^2} + \frac{m\left(C_r \cdot l_r - C_f \cdot l_f\right)}{2C_f \cdot C_r\left(l_f + l_r\right)}\right) \tag{3.41}$$

Chapter 4

Evaluation

The proposed automated driving control algorithm has been evaluated via computer simulations and vehicle tests. The commercial vehicle software, CarSim, and MATLAB/Simulink has been used for the mathematical simulation. In order to show the effectiveness of the proposed algorithm, the simulation scenario has been developed to imitate a multi-traffic driving situation which could commonly happen in a real world. The vehicle tests have been conducted on the actual roads, which are the circular road of Seoul national university and Yongin-Seoul motorway for representing complex driving environment and high speed driving environment respectively, to show the similarity between the driving characteristics of human drivers and that of the proposed algorithm.

4.1 Performance Evaluation via Simulation with Multi-traffic Driving Environment

The first simulation scenario is depicted as shown in Figure 4.1. A subject vehicle follows a preceding vehicle with pre-defined time gap. The vehicles driving in the adjacent lane (depicted as red and blue vehicle) try to change its lanes to the subject vehicle's lane without noticing the existence of subject vehicle.

Figure 4.1. Simulation Scenario

A risk potential function assesses the desired motion of the subject vehicle for avoiding collision with adjacent vehicles.

The first step for the desired motion determination is to assess whether the current collision risk is avoidable without braking. If the current collision risk can be avoidable without braking, then the lateral acceleration profile is calculated to satisfy both avoiding the collision with the preceding vehicle and keeping its lane. The following figure depicts the avoiding motion of the subject vehicle and lateral clearance between the subject vehicle and adjacent vehicles. The desired motion command generated from the risk potential function has been confirmed to keep the lateral safety margin for avoiding collision.

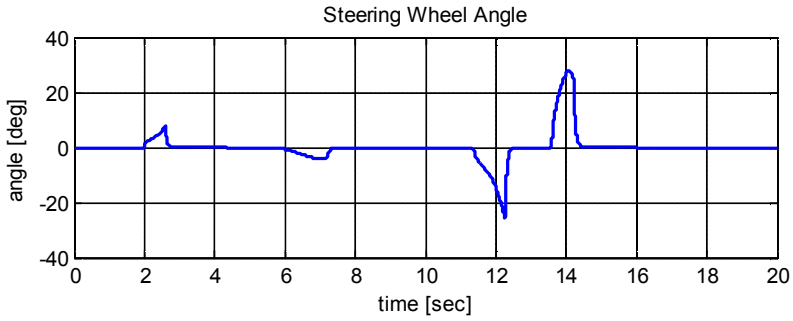

(a) Cabin Steering Wheel Angle of the Subject Vehicle

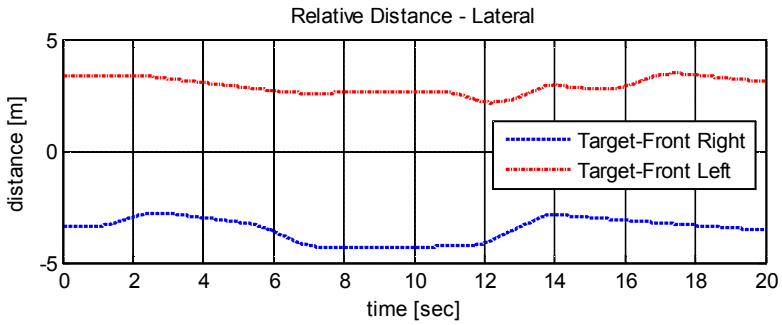

(b) Lateral Clearance with Adjacent Vehicles

Figure 4.2. Vehicle Steering Control with Lane Keeping Simulation Results

The second simulation results indicating the time history of the vehicle behavior are depicted as shown in Figure 4.3. The preceding vehicle drives at 80km/h keeping its lane with 70m of initial clearance to the subject vehicle, which cruises at 105km/h set speed. The risk potential function assesses the desired motion of the subject vehicle for collision avoidance with proceeding vehicle. The first step for the desired motion determination is to assess whether the current collision risk is avoidable without braking. If the current collision risk can be avoidable without braking, then the lateral acceleration

profile is calculated to satisfy both avoiding the collision with the preceding vehicle and preventing the lateral collision with adjacent vehicle as shown in Figure 4.4.

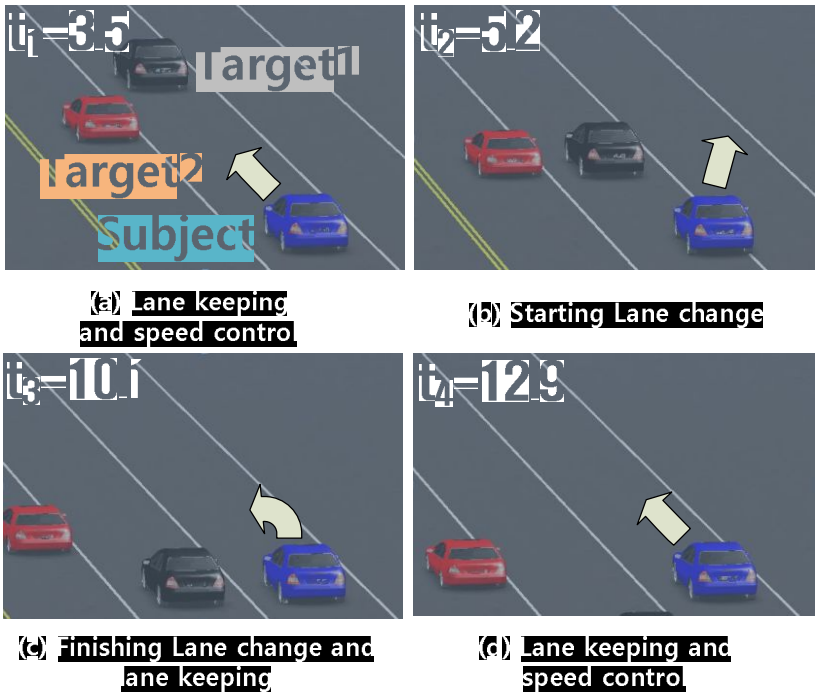

Figure 4.3. Lane Keeping and Lane Change Control Sequence

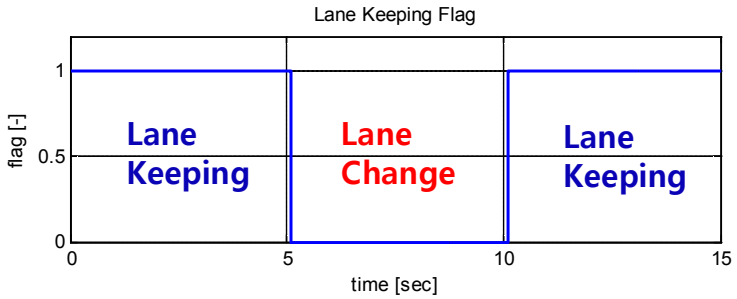

(a) Driving Mode Transition

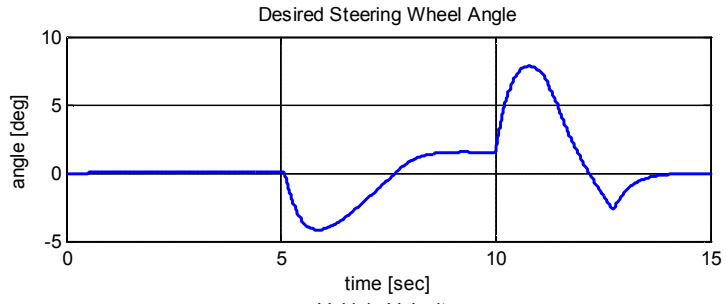

(b) Desired Steering Wheel Angle

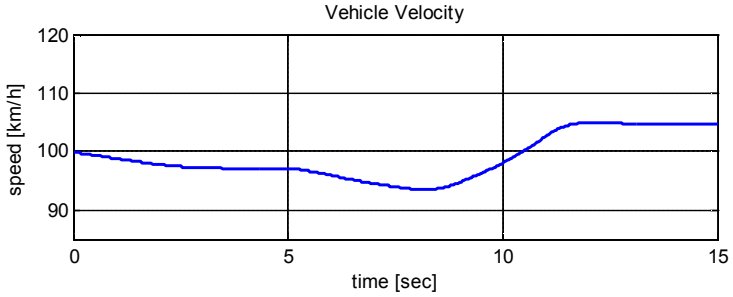

(c) Velocity Profile of a Subject Vehicle

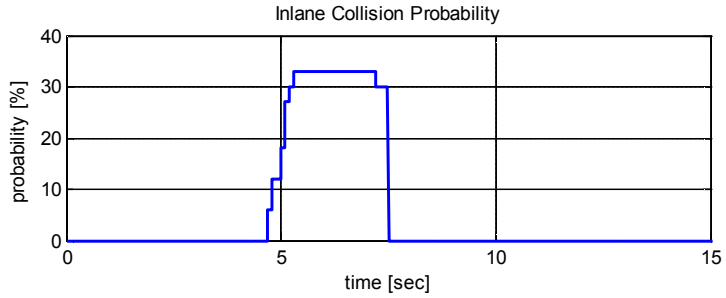

(d) Collision Probability of Inlane Target (Target1)

Figure 4.4. Lane Keeping and Lane Change Simulation Results

4.2 Performance Evaluation via Test Vehicle

A proposed algorithm has been implemented on a developed test vehicle. Since the main purpose of the algorithm is to use vehicle sensor and commercialized sensors which are radar, vision and low cost GPS, the test vehicle has been developed based on its default functionality such as adaptive cruise control and radar, lane departure warning and vision sensor, and motor driven power steering. Based on these advanced driver assistance system, the developed algorithm intervenes its default function only as an actuator. The tests have been conducted on the test track and actual roads, which are the circular road of Seoul national university and Yongin-Seoul motorway for representing complex driving environment and high speed driving environment respectively, to show the similarity between the driving characteristics of human drivers and that of the proposed algorithm. The algorithm has been implemented on a commercial electronic control unit (ECU), and it has been verified the real-time performance of the developed algorithm even on ECU, not only on a rapid control prototype (RCP) such as Autobox.

4.2.1 Test Vehicle Configuration

In order to evaluate the proposed algorithm on a real test vehicle, Hyundai-Kia Motors K7 is used as a test vehicle platform. Figure 4.5 shows the test vehicle configuration. In order to measure DLC, heading angle and road curvature, a Mobileye camera system is equipped on the test vehicle. The proposed algorithm has been implemented on "dSPACE Autobox", which is used for the real-time application and equipped with a DS1005 processor board. Delphi radars are equipped on the test vehicle to perceive surrounding environments. The hardware components mentioned above communicate through a CAN bus.

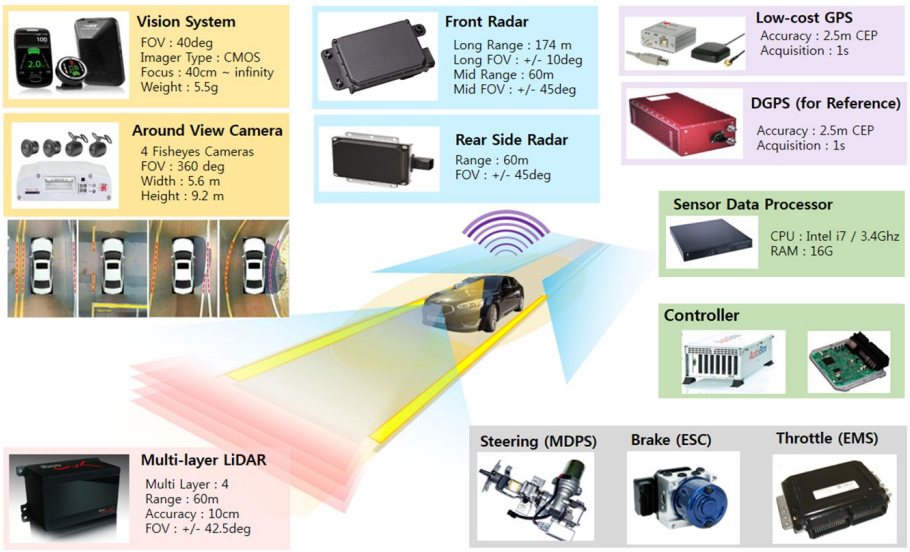

Figure 4.5. Test Vehicle Configuration

4.2.2 Vehicle Tests

Vehicle tests have been conducted for several times at the circular road of Seoul National University. The details of test roads are depicted in Figure 4.6. The given test roads have quite complicated environments to drive automatically (Figure 4.6(b)) along with the test route depicted in Figure 4.6(a). The lanes were hard to be distinguished because of faded paint. There are a lot of buses parked along the road as shown in Figure 4.6(c). In Figure 4.6(d), there exist non-vehicle obstacles such as pedestrian and guardrail. Also, we need to consider other traffic participants like oncoming and preceding vehicles as described in Figure 4.6(e).

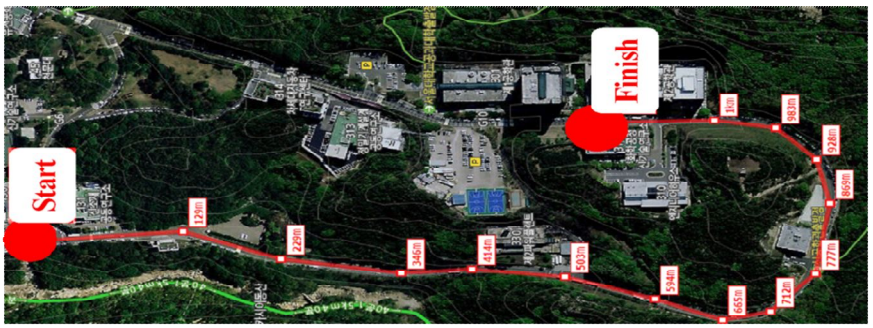

(a) Test routes in SNU

(b) Inside of test vehicle

(c) Highly extreme condition

(d) Non-vehicle obstacles (e) Other traffic participants

Figure 4.6. Configuration of Urban Test Road

The proposed automated driving algorithm has shown the satisfactory control performance and the test results are given in Figure 4.6. As shown in Figure. 13, the ego-vehicle drives through a narrow urban surround with static infrastructure (buildings, trees, poles, etc.), parking cars on the right as well as a preceding vehicle. Consequently, the test vehicle successfully completed the test route with the proposed automated driving algorithm.

Figure 4.7 shows details of test results of the given scenario depicted in Figure 4.6. The vertical magenta bar in Figure 4.7(a) and (b) represents the static obstacles which are parked bus around a subject vehicle. A dynamic drivable area has been determined from the detected static obstacles and center line of the road, which represent the right and left boundary of the drivable area. The magenta line on a road in Figure 4.7(a) represents the center of left and right boundary of dynamic drivable colored with green area. The most intuitive way to guarantee the safety driving within the dynamic drivable area is tracking the center of the drivable area. However, when the vehicle follows the centerline of the drivable area, a driver may feel

uncomfortable because of the overacted control input which is too large or too frequent, for the sensor uncertainties. The manual driver's steering input and the centerline tracking have been compared in Figure 4.7(c). A proposed predictive risk potential based driving control algorithm and manual steering input has been depicted in Figure 4.7(d). A control input from the proposed automated driving control algorithm within the dynamic drivable area shows moderate maneuver which has smaller magnitude and frequency than centerline tracking method, and it reveals that the proposed control algorithm has more correlation with an actual driver's pattern, and guarantees its safety within safety driving envelope represented with green area in Figure 4.7(a). When a preceding vehicle appears as shown in Figure 4.6(e), the subject vehicle keeps the lane and maintains below 20% of maximum collision probability with the preceding vehicle within a future time horizon of 2seconds as shown in Figure 4.7(e).

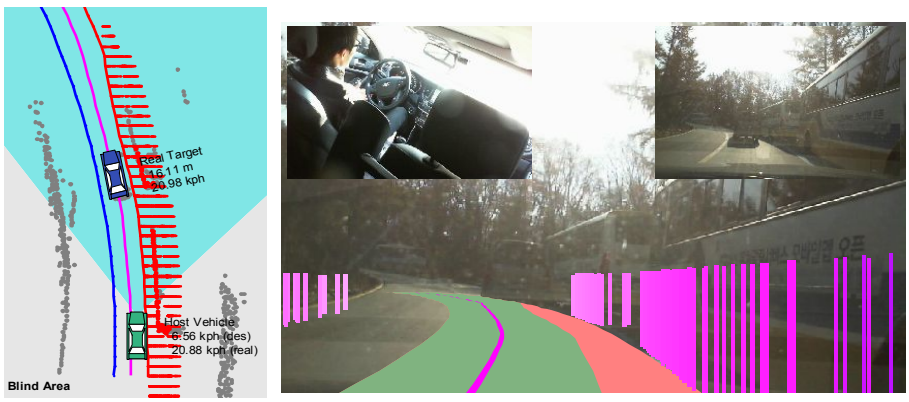

(a) Bird's eye view (b) Driver view

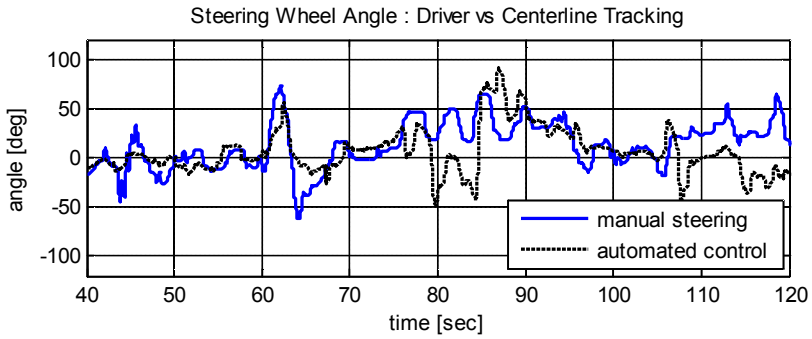

(c) Centre line tracking method with actual driver command

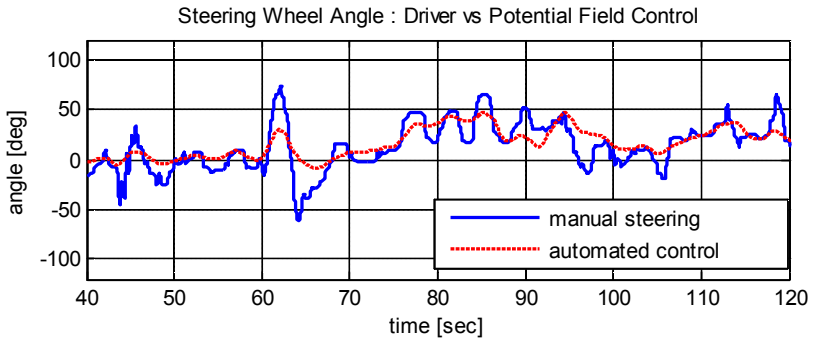

(d) Potential field based control method with actual driver command.

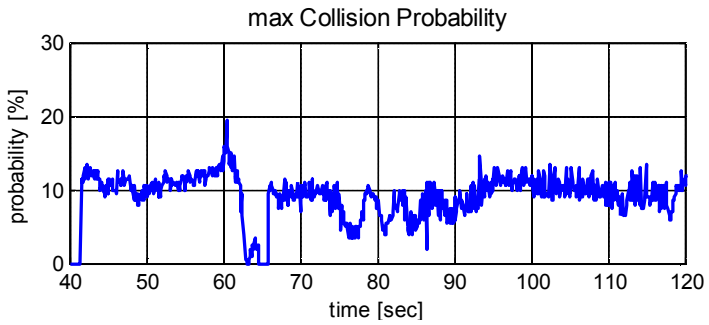

(e) Time History of Maximum collision probability within a time horizon of 2seconds

Figure 4.7. Vehicle Test Results in Urban Road

In the case of preceding vehicle following, a subject vehicle maintains its safety clearance by speed control. A desired acceleration from the developed safety control algorithm has been verified via vehicle test as shown in Figure 4.8. From the test results, a vehicle keeps its lane with steering control, and it is verified to have smoother deceleration profiles which provides a good ride feel to a driver.

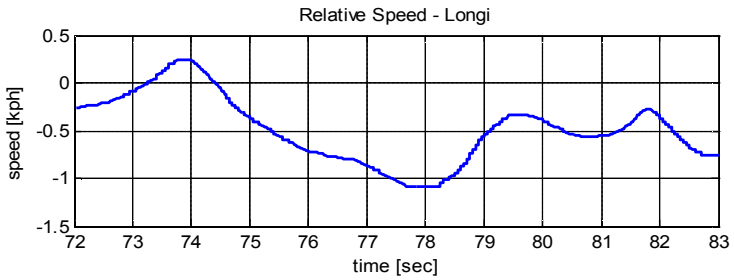

(a) Longitudinal Relative Velocity

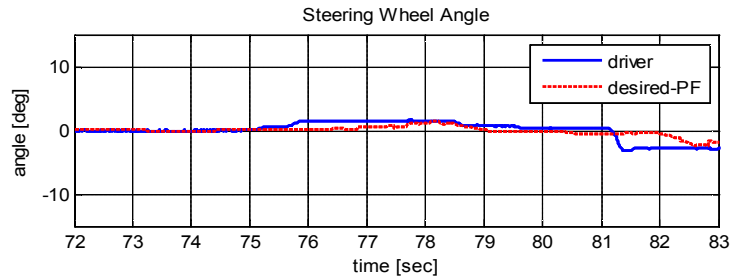

(c) Steering Wheel Angle

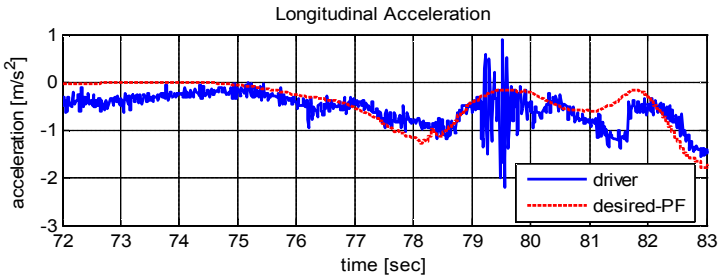

(d) Longitudinal Acceleration

Figure 4.8. Desired Command Validation via Test Data

A centerline tracking-based automated driving control algorithm and a proposed predicted potential-risk based automated driving control algorithm can be compared as shown in Table 2 and Figure 4.9. A minimum clearance with the static obstacle around a subject vehicle has been reduced via the proposed automated control algorithm, however, the maximum lateral acceleration and the maximum side slip angle has been reduced more than 20%, which represent a ride comfort to a driver and lateral stability of the subject vehicle, respectively.

Table 2. Performance Comparison of Centreline Tracking and Predicted Potential Field-based Automated Control in Urban Road

Objective	Evaluation Index	Centerline Tracking-based Automated Control	Potential Field-based Automated Control	Improvement
Safety	$\min C_{y,obstacle}$	73.58cm	67.52cm	**-8.23%**
Ride Comfort	Maximum Lateral Acceleration	1.27m/s^2	0.94m/s^2	**25.98%**
Stability	$\max \lvert\beta\rvert$	0.049deg	0.038deg	**22.45%**

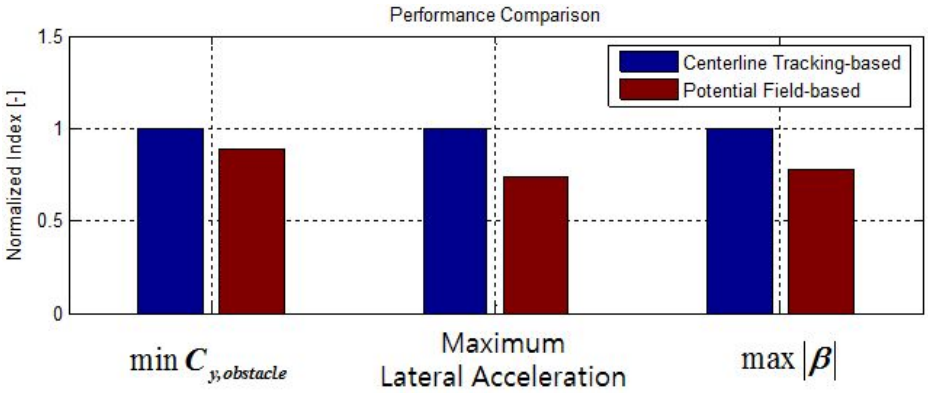

Figure 4.9. Normalized Performance Index in Urban Road

In a high speed driving in motorway, the same algorithm has been implemented. Figure 4.10(a) shows details of the given test scenario on motorway. A safety envelope of the scenario is represented as Figure 4.10(a) with green area. Figure 4.10(b) represents the comparison results with centre line tracking which follows the centre of the green area and proposed automated driving control algorithm. Since there are few disordered static obstacle in the side of the road, and it has relatively small curvature, the

steering behavior in high speed driving is less frequent and has smaller magnitude than an urban driving. The comparison results reveals that the proposed control algorithm shows the moderate control input considering a driver's pattern and at the same time, guaranteeing a safety driving within the safety driving envelope even in the high speed under 35 % of collision probability as shown in Figure 4.10(d).

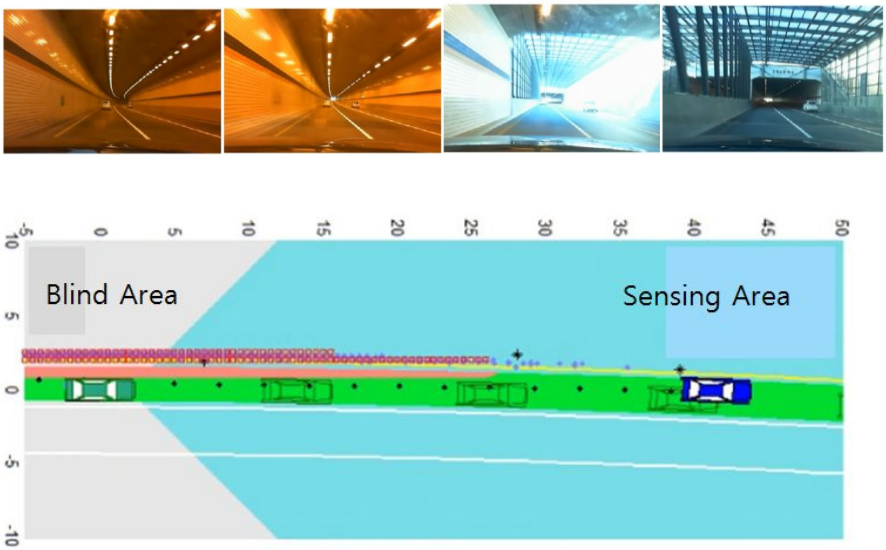

(a) Visual Outline of the surround recognition on motorway

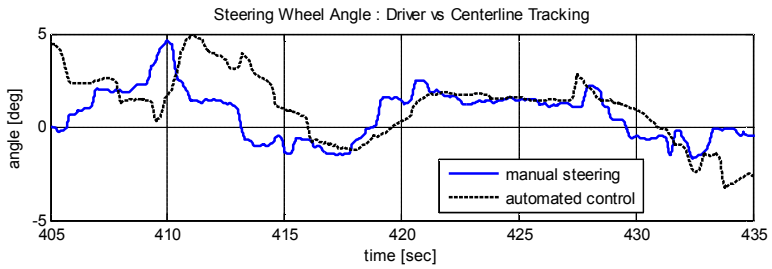

(b) Centre line tracking method with actual driver command

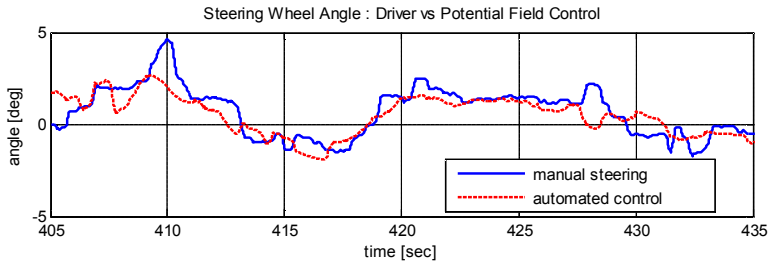

(c) Potential field based control method with actual driver command

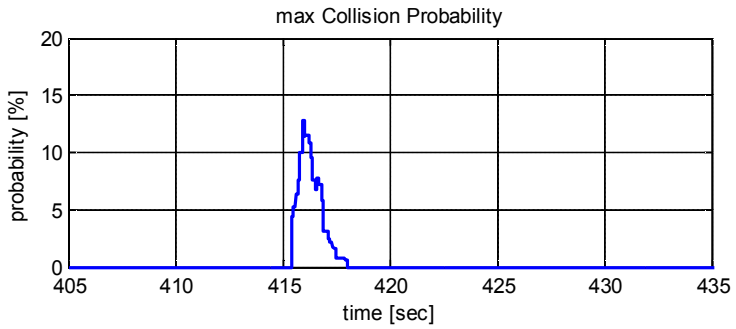

(d) Time History of Maximum collision probability within a time horizon of 2seconds

Figure 4.10. Vehicle Test Results in Motorway

A centerline tracking-based automated driving control algorithm and a proposed predicted potential-risk based automated driving control algorithm in high speed driving situation has been compared as shown in Table.3 and Figure 4.11. A minimum clearance with the static obstacle around a subject vehicle has been reduced via the proposed automated control algorithm, for the centerline tracking always remains the safety clearance of the half width of the safety driving envelope, however, the maximum lateral acceleration and

the maximum side slip angle has been reduced more than 20% as the same with the urban driving test, which represent a ride comfort to a driver and lateral stability of the subject vehicle, respectively.

Table 3. Performance Comparison of Centreline Tracking and Predicted Potential Field-based Automated Control in Motorway

Objective	Evaluation Index	Centerline Tracking-based Automated Control	Potential Field-based Automated Control	Improvement
Safety	$\min C_{y,object}$	135.15cm	121.78cm	**-9.89%**
Ride Comfort	Maximum Lateral Acceleration	1.52m/s^2	1.19m/s^2	**21.71%**
Stability	$\max \lvert\beta\rvert$	0.057deg	0.041deg	**28.07%**

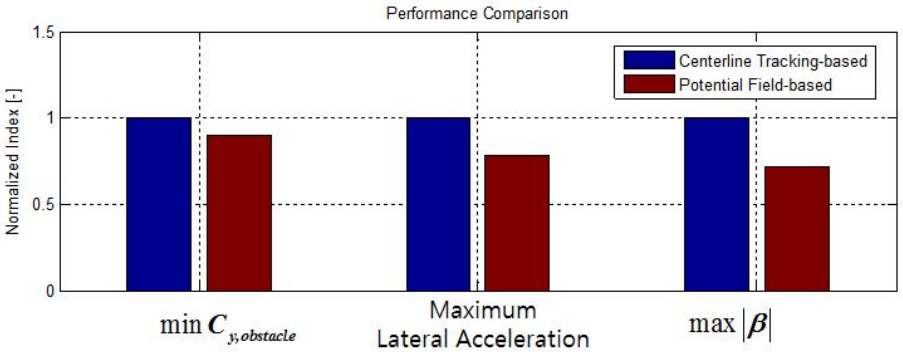

Figure 4.11. Normalized Performance Index in Motorway

Chapter 5

Conclusions and Future Works

Design, real-time implementation and test of dynamic driving control of automated vehicle based on integrated risk management have been presented in this dissertation. The proposed algorithm consisted of the following three steps: an integrated risk assessment, vehicle motion control, and evaluation via mathematical simulations and vehicle tests. In the integrated risk assessment, nonlinear estimation method, such as Extended Kalman Filter (EKF) has been adopted for estimating vehicle longitudinal and lateral velocity estimation algorithm using a low-cost GPS and vehicle sensor. The probabilistic prediction method has been adopted to represent the future collision risk between a subject and surrounding vehicles using the estimated states, and the collision probability has been defined using the predicted motions of the vehicles. For the surround recognition, algorithms for static/moving obstacle detection, and dynamic drivable area representation for the safety of automated driving has been developed. A motion control based on predicted motion of a host vehicle and around vehicle and its predicted

potential risk has been developed within a dynamic driving envelope. In order to guarantee the safety driving, the dynamic driving envelope has been set to be a boundary of the controlled motion. Yaw rate candidates and longitudinal acceleration candidates are developed within the dynamic driving envelope, considering the stability constraints of the vehicle which should be guaranteed for the lateral stability. Each desired motion candidate are propagated within the future time horizon, and the desired motion at each time step is selected from the predefined performance function minimizing the magnitude of the control input, the rate of change of the control input and predicted potential risk function around the subject vehicle.

The performance of the proposed automated driving algorithm has been evaluated via test-data based simulations using CarSim and MATLAB/Simulink and vehicle tests. The simulation results revealed that the proposed collision avoidance algorithm prevents the collision with the surrounding vehicles. From the test data, the desired motion calculated from the integrated safety control algorithm is shown to be similar to actual command of a driver, in other words, the control input from the proposed algorithm could reflect human driver's driving characteristics. It has been shown that proposed automated driving algorithm which has been successfully implemented on real-time electronic control unit (ECU) can provide the robust performance on an urban scenario and high speed motorway.

In the future, evaluations under more various road conditions, and traffic situations should be conducted for the verification of the reliability of the

proposed algorithm. In addition, a research for the extension of the operating region of the proposed algorithm to guarantee all-around automated driving performance should be considered in the future.

Bibliography

[Ge 02] S. Ge and Y. Cui, “Dynamic Motion Planning for Mobile Robots Using Potential Field Method,” Autonomous Robots, Vol. 13,pp.207-222, 2002

[Matsumi 13] Ryosuke Matsumi, Pongsathorn Raksincharoensak, Masao Nagai, “Autonomous Braking Control System for Pedestrian Collision Avoidance by Using Potential Field”, Proceedings of the 7TH IFAC Symposium on Advances in Automotive Control, 2013

[Shimoda 07] Shingo Shimoda, Yoji Kuroda and Karl Iagnemma, “Potential Field Navigation of High Speed Unmanned Ground Vehicles on Uneven Terrain”, Proceedings of the 2005 IEEE International Conference on Robotics and Automation, 2005

[Polychronopoulos 07] Polychronopoulos, A. Tsogas, M., Amditis. A.J., Andreone, L., "Sensor Fusion for Predicting Vehicles' Path for Collision Avoidance Systems," Intelligent Transportation Systems, IEEE Transactions on , vol.8, no.3, pp.549-562, Sept. 2007.

[Yi 04] Kyongsu Yi, Il-Ki Moon, "A driver-adaptive stop-and-go Cruise control strategy," Proceedings of the 2004 IEEE International Conference on Networking, Sensing and Control, 2004

[NHTSA 07] National Highway Traffic Safety Administration, “Pre-Crash Scenario Typology for Crash Avoidance Research”, 2007

[Balcones 09] D. Balcones et al., “Real-Time Vision-Based Vehicle Detection

for Rear-End Collision Mitigation Systems", Computer Aided Systems Theory - EUROCAST 2009, Vol(5717), 2009, pp. 320-325

[Fancher 00] P. Fancher et al., "Human-centered design of an ACC-with-braking and forward-crash-warning system", Proceeding of AVEC2000, 5th International Symposium on Advanced Vehicle Control, Ann Arbor, Michigan, USA, 2000.

[Cho 10][Cho 10] Wanki Cho, Seungwuk Moon, Sihyoung Lee, and Kyongsu Yi, 2010, "Intelligent Vehicle Safety Control Based on Index plane",AVEC 2010

[Moon 08] Seungwuk Moon, Kyongsu Yi, "Human driving data-based design of a vehicle adaptive cruise control algorithm", Vehicle System Dynamics, 2008, Vol.8, No.4, pp.661-690

[Liu 00] Liu Chengqing, Marcel0 H Ang Jr, Hariharan Krishnan, Lim Ser Yong, "Virtual Obstacle Concept for Local-minimum-recovery in Potential-field Based Navigation", Proceedings of 2000 IEEE International Conference on Robotics & Automation, 2000

[Takahiro 14] Takahiro Hasegawa, Pongsathorn Raksincharoensak and Masao Nagai, "Risk-Potential Based Motion Planning and Control of Proactive Driving Intelligence System for Enhancing Active Safety", Proceedings of the AVEC'14, 2014

[Rossetter 05] Eric J. Rossetter and J. Christian Gerdes, "Lyapunov Based Performance Guarantees for the Potential Field Lane-keeping Assistance System", Journal of dynamic systems, measurement and control, 128(3), pp. 510-522, 2005

[Matthew 06]Matthew Spenko, Yoji Kuroda Steven Dubowsky and Karl

Iagnemma, “Hazard avoidance for high-speed mobile robots in rough terrain”, Journal of Field Robotics, Vol. 23, pp. 311–331, 2006

[Yoon 07] Jangyeol Yoon, Dongshin Kim and Kyongsu Yi, “Design of a rollover index-based vehicle stability control scheme”, Vehicle System Dynamics, Vol. 45, pp. 459-475, 2007

[Kim 13] Beomjun Kim and Kyongsu Yi, “Probabilistic States Prediction Algorithm using Multi-sensor Fusion and Application to Smart Cruise Control System”, Proceedings of the 2013 IEEE Intelligent Vehicles Symposium, 2013

[Schwartz 03] Schwartz, D.A., "Clothoid road geometry unsuitable for sensor fusion clothoid parameter sloshing", Proceedings of the 2003 IEEE Intelligent Vehicles Symposium, 2003

[RE 60] K. RE, "A New Approach to Linear Filtering and Prediction," Transection of the ASME-Journal of Basic Engineering, pp. 35-45, 1960.

[Furgale 13] P. Furgale, U. Schwesinger, M. Rufli, W. Derendarz, H. Grimmett, P. Muhlfellner, et al., "Toward automated driving in cities using close-to-market sensors: An overview of the V-Charge Project," in Intelligent Vehicles Symposium (IV), 2013 IEEE, 2013, pp. 809-816.

[Rossetter 06] E. J. Rossetter, and J. C. Gerdes, “Lyapunov based performance guarantees for the potential field lane-keeping assistance system”, Journal of Dynamic Systems, Measurement, and Control, Vol. 128, No. 3, pp. 510-522, 2005.

[Sattel 08] T. Sattel, and T. Brandt, “From robotics to automotive: lane-keeping and collision avoidance based on elastic bands”, Vehicle System Dynamics, Vol. 46, No. 7, pp. 597-619, 2008.

[Talvala 11] K. L. R. Talvala, K Kritayakirana, J. C. Gerdes, “Pushing the limits: from lane keeping to autonomous racing”, Annual Reviews in Control, Vol 35, No. 1, pp. 137-148, 2011.

[Naranjo 08] J. E. Naranjo, C. Gonzalez, R. Garcia, and T. Pedro, “Lane-change fuzzy control in autonomous vehicles for the overtaking maneuver”, IEEE Transactions on Intelligent Transportation System, Vol. 9, No. 3, pp. 438-450, 2008.

[Yoon 09] Y. Yoon, J. Shin, H. Kim, Y. Park, and S. Sastry, “Model-predictive active steering and obstacle avoidance for autonomous ground vehicles”, Control Engineering Practice, Vol. 17, No. 7, pp. 741-750, 2009.

[Borrelli 05] F. Borrelli, P. Falcone, T. Keviczky, J. Asgari, and D. Hrovat, “MPC-based approach to active steering for autonomous vehicle systems”, International Journal of Vehicle Autonomous Systems, Vol. 3, No.2, pp. 265-291, 2005.

[Falcone 07] P. Falcone, F. Borrelli, J. Asgari, H. E. Tseng, and D. Hrovat, “Predictive active steering control for autonomous vehicle systems”, IEEE Transactions on Control System Technology, Vol. 15, No. 3, pp. 566-580, 2007.

[Falcone 08] P. Falcone, F. Borrelli, H. E. Tseng, J. Asgari, and D. Hrovat, “Linear time-varying model predictive control and its application to active steering systems: Stability analysis and experiment validation”, International Journal of Robust and Nonlinear Control, Vol. 18, No. 8, pp. 862-875, 2008.

[Althoff 09] M. Althoff, O. Stursberg, and M. Buss, “Model-based probabilistic collision detection in autonomous driving”, IEEE Transactions on Intelligent Transportation System, Vol. 10, No. 2, pp. 299-310, 2009.

[Ferguson 13] D. Ferguson, and D. Dolgove, “Modifying behavior of autonomous vehicle based on predicted behavior of other vehicles”, Pat. no. 20130261872A1, United States, 2013.

[Cho 10-1] Wanki Cho, Jangyeol Yoon, Seongjin Yim, Bongyeong Koo and Kyongsu Yi, “Estimation of Tire Forces for Application to Vehicle Stability Control”, IEEE Transactions on Vehicular Technology, Vol.59, No.2, pp. 638-649, 2010

[Cho 10-2] Wanki Cho, Seungwuk Moon, Sihyoung Lee, and Kyongsu Yi, 2010, "Intelligent Vehicle Safety Control Based on Index plane",AVEC 2010

[Moustapha 09] Moustapha Doumiati, Alessandro Victorino, Ali Charara and Daniel Lechner, “Unscented Kalman filter for real-time vehicle lateral tire forces and sideslip angle estimation”, Intelligent vehicles symposium, 2009 IEEE, pp. 901-906, June , 2009

[Guillaume 06] Guillaume Baffet, Ali Charara and Joanny St´ephant, “Sideslip angle, lateral tire force and road friction estimation in simulations and experiments”, Proceedings of the 2006 IEEE International Conference on Control Applications, pp. 903-908, October 4-6, 2006

[Ray 97] Ray, L R., “Non-linear tyre force estimation and road friction identification: simulation and experiments”, Automatica, Vol. 33, No. 10, pp. 1819-1833, 1997.

[Rajesh 06] Rajesh Rajamani, “Vehicle Dynamics and Control”, Springer, pp. 15-47 and pp. 220-256, 2006

[Lee 11] Taeyoung Lee, Beomjun Kim, Kyongsu Yi and Changhyun Jeong, “Development of Lane Change Driver Model for Closed-loop simulation of the Active Safety System”, 14th IEEE International Intelligent Transportation

Systems Conference (ITSC), The George Washington University (GWU) at Washington, DC, October 5-7, 2011

[Fancher 00] P. Fancher et al., “Human-centered design of an ACC-with-braking and forward-crash-warning system”, Proceeding of AVEC2000, 5th International Symposium on Advanced Vehicle Control, Ann Arbor, Michigan, USA, 2000.

[Kaempchen 09] Kaempchen, N., Schiele, B., Dietmayer, K., "Situation Assessment of an Autonomous Emergency Brake for Arbitrary Vehicle-to-Vehicle Collision Scenarios," Intelligent Transportation Systems, IEEE Transactions on , vol.10, no.4, pp.678-687, Dec. 2009

[Jansson 04] Jansson, J., “Dealing with uncertainty in automotive collision avoidance,” in Advanced Microsystems for Automotive Applications. Berlin, Germany: Springer-Verlag, pp. 165–180, 2004

[Lambert 08] Lambert, A., Gruyer, D., Pierre, G.S., Ndjeng, A.N., “Collision Probability Assessment for Speed Control”, Intelligent Transportation Systems, 2008. ITSC 2008. 11th International IEEE Conference on ,vol., no., pp.1043-1048, 12-15 Oct. 2008

[Karlsson 08] Karlsson, R., Jansson, J. and Gustafsson, F.; , “Model-based statistical tracking and decision making for collision avoidance application,” in Proc. Amer. Control Conf., Jun. 30–Jul. 2, vol. 4, pp. 3435–3440, 2004

[Sandblom 11] Sandblom, F., Brannstrom, M., "Probabilistic threat assessment and driver modeling in collision avoidance systems", Intelligent Vehicles Symposium (IV), 2011 IEEE, pp. 914 - 919, 2011

[Broadhurst 05] Broadhurst, A., Baker, S., Kanade, T., "Monte Carlo road safety reasoning", Intelligent Vehicles Symposium, 2005. Proceedings. IEEE ,

vol., no., pp. 319- 324, 6-8, 2005

[Mammar 06] Said Mammar, Sebastien Glaser and Mariana Netto, “Time to Line Crossing for Lane Departure Avoidance: A Theoretical Study and an Experimental Setting”, IEEE Transactions on Intelligent Transportation Systems, Vol.7, No.2, pp. 226-241, 2006

초 록

통합 예측 위험 관리 기반 포텐셜 필드 기법을 이용한 자율 주행 제어 알고리즘 개발

전 세계적으로 차량 판매량이 연간 6천만대를 돌파하며 자동차 시장의 규모가 점차 증대됨에 따라 자동차 관련 기술의 발전이 가속화되고 있다. 운전자 편의를 위해 장착된 네비게이션 시스템, DMB, 스마트폰 등 편의 장비들의 보급이 활발히 이루어졌으나, 이러한 편의 장비들의 운전 중 조작이나 졸음 등에 기인한 운전 집중력 하락은 전체 사고 원인의 약 90%를 차지하고 있다. 이를 위해 다양한 운전자 지원 시스템(ADAS : Advanced Driver Assistance System)이 개발되었으며, 크게 차선 이탈과 관련된 차선 이탈 경보장치(LDWS : Lane Departure Warning System), 차선 유지 보조 장치(LKAS : Lane Keeping Assistance System), 사각 지대 감지 장치(BSD : Blind Spot Detection) 등의 횡방향 안전 기술과 적응형 순항 제어 시스템(ACC : Adaptive Cruise Control), 긴급 비상 제동 제어 시스템(AEB : Advanced Emergency Braking) 등의 종방향 안전 기술이 차량에 양산 적용되고 있다. 최근에는 이러한 개별 안전 보조 장치의 통합화가 진행 중이며, 궁극적으로 전(全) 방향에 대한 안전을 확보하며, 운전 중 운전자에게 최대한의 편의를 제공하는 무인 자율 주행 차량에 대한 연구가 활발히 이루어지고 있다.

본 논문에서는 현재까지 양산되었거나 양산 가능성이 있는 레이더, 카메라 센서, 저가형 GPS 기반의 플랫폼에서 자율 주행을 구현하는 주행 제어 알고리즘을 제안하였다. 전체 주행 알고리즘은 주행 상태 추정 및 차량 거동 예측, 차량 거동 예측에 따른 주행 안전 영역 구성, 운전자 승차감 및 안전 확보를 위한 주행 안전 영역 내 주행 제어 알고리즘으로 구성된다.

기존의 종방향 및 횡방향 개별 안전 보조장치의 작동 시점과 제어 정도를 결정하는 개별 충돌 위험도를 통합한 확률적 충돌 위험 예측을 위해 주행 상태 추정, 차량 거동 예측, 예측된 거동에 대한 충돌 위험도 판단을 도입하였고, 이를 기반으로 유한 시간 영역 내의 자차량 및 주변 주행 차량의 미래 거동을 예측하여 자차량의 주행 안전 영역을 정의하였다. 주행 안전 영역 내에서의 주행 제어를 위해 유한 시간내의 예측된 위험 포텐셜 필드 기법이 사용되었으며, 운전자의 운전 이질감 및 위험도가 최소화될 수 있는 목적함수를 정의하고, 이를 최소화하는 종방향 목표 가속도 및 목표 조향각을 결정하였다.

제안된 자율 주행 제어 알고리즘의 성능은 시뮬레이션과 실차 실험을 통해 검증되었다. 시뮬레이션은 MATLAB/SIMULINK 및 차량 동역학 시뮬레이션 전용 SW인 CARSIM에 기반하여 수행하으며, 본 연구에서 제안된 자차량 및 주변 차량의 확률적 거동 예측 기반 자율 주행 제어 알고리즘의 유효성을 검증하기 위해서 실 도로상에서 발생할 수 있는 다차량 주행 시나리오를 구성하여 성능을 검증하였고, 감속, 차선 내 조향 및 차선 변경을 통한 안전 확보 성능을 확인하였다. 나아가 운전자의 실제 제어

경향과 제어 알고리즘의 제어 경향성 일치를 위해 실도로 상에서 개발된 자율 주행 시험 차량을 통한 실차 검증을 수행하였으며, 본 연구에서 제안된 예측 위험 포텐셜 필드 기반 주행 알고리즘이 안전 영역 내 중앙 경로 추종 알고리즘에 비해 안전 확보 성능을 향상시키고 운전자의 승차감을 향상시키는 효과가 있음을 확인하였다. 또한 본 연구에서 구현된 예측 위험 포텐셜 필드 기반 자율 주행 알고리즘은 기존의 모델 예측 기반 자율 주행 알고리즘에 비해 적은 계산량으로 고가의 실시간 자동 코딩 제어기(RCP : Rapid Control Prototype) 뿐 아니라 상용화된 차량용 전용제어기(ECU)에서도 적용이 가능함을 실차 테스트를 통해 확인하였다.

주요어: 차량 상태 추정, 차량 상태 예측, 예측 충돌 위험도, 포텐셜 필드, 운전자 주행 특성

학 번: 2011-30197